

Effects of tau-neutrino detection on non-standard interactions at DUNE with a short discussion on the nature of neutrino mixing

Xin Yue Yu, Zishen Guan, William Dallaway, Ushak Rahaman, Nikolina Ilic,

Department of Physics, University of Toronto, Toronto, ON M5S 1A7, Canada

E-mail: xyz.yu@mail.utoronto.ca, nick.guan@mail.utoronto.ca,
william.dallaway@mail.utoronto.ca, ushak.rahaman@cern.ch,
Nikolina.Ilic@cern.ch

ABSTRACT: In this paper, we investigate the effects of ν_τ and $\bar{\nu}_\tau$ detection at the DUNE far detector on the experiment's sensitivity to Non-Standard Interactions (NSI) in neutrino propagation. We show that the strongest observable NSI effect in the ν_τ and $\bar{\nu}_\tau$ appearance probabilities arises from $\epsilon_{\mu\tau}$. We have studied the hierarchy sensitivity, CP violation sensitivity and octant sensitivity of DUNE from ν_τ and $\bar{\nu}_\tau$ appearance channels in presence of NSI. We have also studied the detection sensitivity of NSI phases and the future constraints on NSI parameters from the tau neutrino appearance channels in DUNE. Additionally, we examine the role of ν_τ detection in constraining the unitary nature of the PMNS matrix. These studies emphasize the importance of incorporating ν_τ detection in long-baseline neutrino experiments such as DUNE.

Contents

1	Introduction	1
2	Theoretical background and motivations	4
3	Simulation details	8
4	Results and discussions	12
4.1	Mass hierarchy sensitivity	16
4.2	CP violation sensitivity	17
4.3	Octant sensitivity	20
4.4	Determining NSI phases	20
4.5	Sensitivity to NSI parameters	25
5	A short discussion on the unitarity of PMNS matrix and role of τ neutrino in determining it	25
6	Conclusions	28
A	More discussions on fluxes and detector simulations	33
B	Octant sensitivity for NSI due to $\epsilon_{\mu\tau}$, $\epsilon_{\mu\mu}$ and $\epsilon_{\tau\tau}$	34
C	Sensitivity to $\epsilon_{e\mu}$ and $\epsilon_{e\tau}$	34

1 Introduction

The neutrino oscillation phenomenon is one of those few windows, in the otherwise complete standard model (SM), which gives the particle physics community an opportunity to look into the promising world of the beyond standard model physics. In the simplest extension of SM, in order to accommodate neutrino oscillation, the neutrino mass and flavour states mix through a unitary transformation, defined by the unitary PMNS mixing matrix

$$U = \begin{pmatrix} c_{13}c_{12} & s_{12}c_{13} & s_{13}e^{-i\delta_{\text{CP}}} \\ -s_{12}c_{23} - c_{12}s_{23}s_{13}e^{i\delta_{\text{CP}}} & c_{12}c_{23} - s_{12}s_{23}s_{13}e^{i\delta_{\text{CP}}} & s_{23}c_{13} \\ s_{12}s_{23} - s_{13}c_{12}c_{23}e^{i\delta_{\text{CP}}} & -c_{12}s_{23} - s_{13}c_{23}s_{12}e^{i\delta_{\text{CP}}} & c_{23}c_{13} \end{pmatrix}, \quad (1.1)$$

where $c_{ij} = \cos\theta_{ij}$, and $s_{ij} = \sin\theta_{ij}$, with $i, j = 1, 2, 3$. Neutrino oscillation probabilities are functions of three mixing angles θ_{12} , θ_{13} , and θ_{23} , one CP violating phase δ_{CP} , and two mass-squared differences $\Delta_{21} = m_2^2 - m_1^2$ and $\Delta_{31} = m_3^2 - m_1^2$. Decades of neutrino oscillation experiments have enabled the particle physics community to measure most of

the neutrino oscillation parameters, except the sign of Δ_{31} , octant of θ_{23} , and δ_{CP} .¹ The current global best-fit values of the neutrino oscillation parameters have been listed in table 1. Depending on the sign of Δ_{31} , there can be two possibilities: 1. Normal hierarchy (NH): $m_3 \gg m_2 > m_1$, and 2. Inverted hierarchy (IH): $m_2 > m_1 \gg m_3$, where m_i s are the mass of the neutrino mass eigenstates ν_i s. Similarly, there can be two possibilities for the octants of θ_{23} : 1. Higher octant (HO): $\sin^2 \theta_{23} > 0.5$, and 2. Lower octant (LO): $\sin^2 \theta_{23} < 0.5$.

The presently running long-baseline accelerator neutrino experiments NO ν A [2] and T2K [3] are expected to measure the unknown neutrino oscillation parameters by measuring the $\nu_\mu \rightarrow \nu_e$ appearance and $\nu_\mu \rightarrow \nu_\mu$ survival probabilities in both neutrino, and anti-neutrino modes. According to the present T2K result [4, 5], $|\Delta_{32}| = (2.494^{+0.041}_{-0.058}) \times 10^{-3} \text{ eV}^2$ ($|\Delta_{31}| = (2.463^{+0.042}_{-0.056}) \times 10^{-3} \text{ eV}^2$), $\sin^2 \theta_{23} = 0.561^{+0.019}_{-0.038}$ ($0.563^{+0.017}_{-0.032}$), $\delta_{\text{CP}} = -1.97^{+0.97}_{-0.62}$ ($-1.44^{+0.56}_{-0.59}$) for NH (IH). On the other hand, the present NO ν A data yields $|\Delta_{32}| = (2.433^{+0.035}_{-0.036}) \times 10^{-3} \text{ eV}^2$ (2.473 ± 0.035), $\sin^2 \theta_{23} = 0.546^{+0.032}_{-0.075}$ ($0.539^{+0.028}_{-0.075}$), $\delta_{\text{CP}}/\pi = 0.88$ (1.51) for NH (IH) [6]. There exists tension between the NO ν A and T2K data regarding the best-fit value of δ_{CP} when the mass hierarchy is normal, and the two experiments rule out the 1σ allowed regions of each other on the $\sin^2 \theta_{23} - \delta_{\text{CP}}$ planes. This tension arises mainly from the $\nu_\mu \rightarrow \nu_e$ appearance channel [7], and has become stronger with time [1]. Several studies have been conducted to resolve this tension with the introduction of beyond standard model (BSM) physics [8–11].

The data collected at future long-baseline accelerator neutrino experiments such as DUNE [12] and T2HK [13] will play a key role to resolving this tension as well as searching for possible BSM physics. Many studies have been conducted on BSM physics in future long-baseline experiments [14–17]. In ref. [10, 11, 18], the authors have explored non-standard interactions (NSI) during neutrino propagation as a possible solution to the tension between NO ν A and T2K. In these references, the effects of NSI in the $e - \mu$ and $e - \tau$ sector have been considered. Since vector NSI results in the addition of a matter-like effect term to the neutrino propagation Hamiltonian, the introduction of NSI does not drastically change the T2K result. This is because for a T2K baseline of 295 km, and flux peaking at an energy of 0.6 GeV, the matter effect in T2K is small and hence the NSI effect is small as well. However, the introduction of NSI in the $e - \mu$ and $e - \tau$ sectors can make significant changes to the oscillation probability $\nu_\mu \rightarrow \nu_e$ ($P_{\mu e}$) and $\bar{\nu}_\mu \rightarrow \bar{\nu}_e$ ($P_{\bar{\mu} \bar{e}}$) and affect the NO ν A result, bringing its best fit point closer to the best fit point of T2K. According to reference [18], for $|\epsilon_{e\mu}| = 0.125$, and $\phi_{e\mu} = 1.35\pi$, NO ν A (T2K) has δ_{CP} best-fit point around 0.9π (1.5π) and both experiments have a large overlap between their allowed regions at 1σ C.L. For $|\epsilon_{e\tau}| = 0.22$, and $\phi_{e\tau} = 1.70\pi$, both experiments have a δ_{CP} best-fit point around 1.5π . Here $\epsilon_{e\mu} = |\epsilon_{e\mu}|e^{i\phi_{e\mu}}$ and $\epsilon_{e\tau} = |\epsilon_{e\tau}|e^{i\phi_{e\tau}}$ are NSI parameters representing the $e - \mu$ and $e - \tau$ sectors respectively.

Looking for $\nu_\mu \rightarrow \nu_\tau$, and $\bar{\nu}_\mu \rightarrow \bar{\nu}_\tau$ oscillations in experiments can provide a useful additional handle in discovering NSI. However, direct measurement of ν_τ events is difficult

¹Readers can see this review article [1] to have an idea about the determination of other neutrino oscillation parameters.

in both beam and atmospheric neutrino oscillation experiments. Neutrino experiments fall into the category of fixed target experiments. This characteristic coupled with a large τ mass yields large threshold energies for ν_τ scattering of ordinary matter. The threshold energy, E_{Th} , is greater than 3.35 GeV (3.1 GeV) for $\nu_\tau + N \rightarrow \tau + N$ ($\nu_\tau + e \rightarrow \tau + \nu_e$), where N is a nucleon [19]. Due the large beam energies of DUNE, motivated by the requirement of observing large Δ_{31} driven oscillations at the far detector, DUNE will be able to observe τ events above this threshold energy. However, the phase suppression effects are large at DUNE, and in its lifetime, the experiment is expected to contain between 100 – 1000 tau events. Moreover, identifying and reconstructing ν_τ events in the liquid argon of the DUNE far detector is challenging, because the decay of a τ lepton involves a ν_τ in the final state, which carries away significant undetectable energy. The beam mode of DUNE, due to its large detector fiducial volume, powerful neutrino beam and exquisite track reconstruction capability, is capable of detecting ν_τ in spite of the challenges. In ref. [20] a novel approach to improving the ν_τ signal (S) over background (B) has been proposed for DUNE. With a τ optimized beam, $S/\sqrt{B} = 8.8$ (11) for hadronic (leptonic) decay of the τ lepton could be achieved in DUNE. In ref. [19, 21], the authors have discussed several physics possibilities with ν_τ in DUNE, including NSI. However, they used an outdated flux prediction, and only addressed the future sensitivity of NSI parameters. In ref. [22], the authors have investigated future sensitivities of the NSI parameters using ν_τ and $\bar{\nu}_\tau$ appearances. However, they also used older flux files, and their detector simulations and energy resolution functions are quite different from our paper. Moreover, in our work, we have investigated the implications of tau neutrino detection at DUNE from theoretical point of view in more details. In the appendix A, we have discussed the relative comparison between the flux files used in this paper and those used in ref. [19, 21, 22].

In this paper, we explore NSI effects with ν_τ in DUNE. We calculate the hierarchy sensitivity, CP violation sensitivity and octant sensitivity of DUNE in presence of NSI. We have considered NSI due to $\epsilon_{e\mu}$ and $\epsilon_{e\tau}$. The presence of these particular values is motivated by the fact that their existence resolves the NO ν A and T2K tension as shown in ref. [10, 11, 18]. We have also considered the effects due to $\epsilon_{\mu\mu}$, $\epsilon_{\mu\tau}$ and $\epsilon_{\tau\tau}$. The detailed physics effects of these parameters on the oscillation probabilities are discussed in the next section. We have also provide future expected constraints on different NSI parameters when the $\nu_\mu \rightarrow \nu_\tau$ oscillation is considered as part of the signal. The issue of determining NSI phases in the case of NSI being present due to either of $\epsilon_{e\mu}$, $\epsilon_{e\tau}$, and $\epsilon_{\mu\tau}$ is also addressed. In section 2, theoretical background and motivations are discussed. The details of analysis, including ν_τ simulation, are discussed in section 3. The final results are provided in section 4. An important physics motivation for the detection ν_τ in DUNE is to constrain the unitary property of the ν_τ mixing with the mass eigenstates. A short discussion on the role of the τ neutrino in determining the unitary property of the PMNS mixing matrix is presented in section 5. The final conclusions are drawn in section 6.

Parameters	NH	IH
$\theta_{12}/^\circ$	$33.68^{+0.73}_{-0.70}$	$33.68^{+0.73}_{-0.70}$
$\theta_{23}/^\circ$	$43.3^{+1.0}_{-0.8}$	$47.9^{+0.7}_{-0.9}$
$\theta_{13}/^\circ$	$8.56^{+0.11}_{-0.11}$	$8.59^{+0.11}_{-0.11}$
$\delta_{\text{CP}}/^\circ$	212^{+26}_{-41}	274^{+22}_{-25}
$\frac{\Delta_{21}}{10^{-5} \text{ eV}^2}$	$7.49^{+0.19}_{-0.19}$	$7.49^{+0.19}_{-0.19}$
$\frac{\Delta_{3l}}{10^{-3} \text{ eV}^2}$	$2.513^{+0.021}_{-0.019}$	$-2.484^{+0.020}_{-0.020}$

Table 1. Best-fit values of the neutrino oscillation parameters according to the present global fits [23, 24]. $\Delta_{3l} = \Delta_{31} > 0$ for NH, $\Delta_{3l} = \Delta_{32} < 0$ for IH.

2 Theoretical background and motivations

In the 3-neutrino paradigm, the $\nu_\mu \rightarrow \nu_\tau$ oscillation probability in vacuum for DUNE with a baseline of 1300 km, and energy above τ threshold ($E > 3.4$ GeV) can be written as

$$\begin{aligned}
P_{\mu\tau}^{\text{vac}} &= 4|U_{\mu 3}|^2|U_{\tau 3}|^2 \sin^2 \left(\frac{\Delta_{31}L}{4E} \right) + \text{subleading} \\
&= \sin^2 2\theta_{23} \cos^4 \theta_{13} \sin^2 \left(\frac{\Delta_{31}L}{4E} \right) + \text{subleading}
\end{aligned} \tag{2.1}$$

Using the best-fit values from ref. [23, 24], we obtain $4|U_{\mu 3}|^2|U_{\tau 3}|^2 \approx 0.95$. The subleading term consists of the solar neutrino oscillation, and an interference term driven by the ratio of two mass-squared differences: $\Delta_{21}/\Delta_{31} \sim 0.03$. This is the major difference with respect to the $\nu_\mu \rightarrow \nu_e$ oscillation probability. In the later case, the leading term is proportional to $|U_{e3}|^2 \approx 0.022$, thus the interference term is of the same order as the leading term.

Throughout our analysis, we have include the matter effect. The matter effect is parameterized by $A = \sqrt{2}G_F n_e E$, where G_F is the Fermi constant, and n_e is the electron density in matter. For DUNE, $A \sim 5.8 \times 10^{-4} E \text{ eV}^2$. Thus, both $\hat{\Delta}_{31} \equiv \Delta_{31}/(2E)$, and $\hat{A} \equiv A/E$ are much larger than $\hat{\Delta}_{21} \equiv \Delta_{21}/(2E)$, for the neutrino energy above 3.4 GeV. Hence, $\hat{\Delta}_{21} \rightarrow 0$ is a good approximation, and under this approximation,

$$P_{\mu\tau} = \sin^2 2\theta_{23} \left| e^{i\frac{\Delta_M L}{2}} \cos^2 \theta_M \sin \left(\frac{\Delta_+ L}{2} \right) + \sin^2 \theta_M \sin \left(\frac{\Delta_- L}{2} \right) \right|^2, \tag{2.2}$$

where

$$\Delta_\pm = \frac{\hat{A} + \hat{\Delta}_{31}}{2} \pm \frac{\Delta_M}{2}, \tag{2.3}$$

$$\Delta_M = \sqrt{(\hat{A} - \hat{\Delta}_{31} \cos 2\theta_{13})^2 + \Delta_{31} \sin^2 2\theta_{13}}, \tag{2.4}$$

$$\tan 2\theta_M = \frac{\hat{\Delta}_{31} \sin 2\theta_{13}}{\hat{\Delta}_{31} \cos 2\theta_{13} - \hat{A}}. \tag{2.5}$$

At the τ threshold energy, $\hat{\Delta}_{31} \approx 3.6/10^{-4} \text{ eV}^2/\text{GeV}$. Thus, $\hat{A} > \hat{\Delta}_{31}$ above the τ threshold energy. In this limit, and when $\hat{\Delta}_{31}L \ll 1$, $\hat{A} \gg \hat{\Delta}_{31}$, eq. 2.2 can be well approximated

by eq. 2.1. In ref. [25], the non-trivial effect of non-zero Δ_{21} have been considered, and it can be seen numerically that the inclusion of matter effect does not change the physics to any significant level.

From eq. 2.1, we can comment that the $\nu_\mu \rightarrow \nu_\tau$ oscillation probability depends on $|\Delta_{31}|$ and $\sin^2 2\theta_{\mu\tau} \equiv |U_{\mu 3}|^2 |U_{\tau 3}|^2 = 1/4 \sin^2 2\theta_{23} \cos^4 \theta_{13}$. Therefore, at the DUNE baseline length, for energies higher than the τ threshold energy, the ν_τ appearance channel does not have hierarchy, δ_{CP} or octant sensitivity. This point has been illustrated in figs. 1-3. From fig. 1, we can see that $P_{\mu\tau}$ is maximum (minimum) for the IH- $\delta_{CP} = 90^\circ$ (NH- $\delta_{CP} = -90^\circ$) hierarchy- δ_{CP} combination. For the anti-neutrino probability $P_{\bar{\mu}\bar{\tau}}$, the opposite holds. Other hierarchy- δ_{CP} combinations fall in between these two extreme cases. However, we can see that above the τ threshold energy of 3.4 GeV, it is difficult to make any significant differentiation between $P_{\mu\tau}$ ($P_{\bar{\mu}\bar{\tau}}$) for the different hierarchy and δ_{CP} combinations.

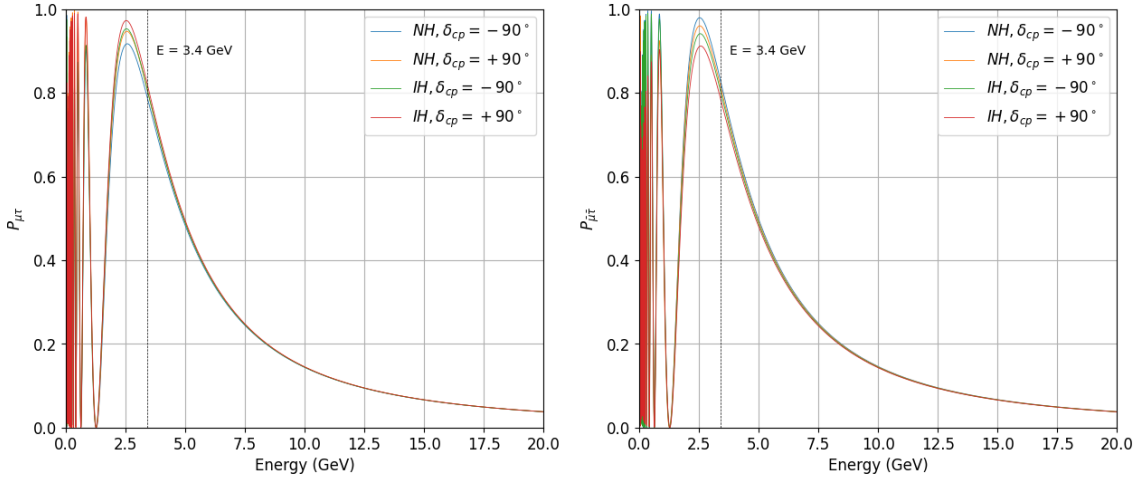


Figure 1. $\nu_\mu \rightarrow \nu_\tau$ oscillation probability as a function of energy with different hierarchy and δ_{CP} values for (anti-) neutrino in the (right) left panel. The hierarchy- δ_{CP} combinations for different coloured lines have been mentioned on the plots. The other oscillation parameters have been fixed to the best-fit values taken from ref. [23, 24].

In fig. 2, we show the oscillation probabilities $P_{\mu\tau}$ and $P_{\bar{\mu}\bar{\tau}}$ for NH- $\delta_{CP} = +90^\circ$ and IH- $\delta_{CP} = -90^\circ$. We have used $\sin^2 \theta_{12} = 0.47$ (0.53) for θ_{23} in LO (HO). At the oscillation probability level, the $\mu - \tau$ oscillation channels do not have any octant sensitivity above the τ threshold energy. Similar conclusions can be drawn from fig. 3 for NH- $\delta_{CP} = -90^\circ$ and IH- $\delta_{CP} = 90^\circ$.

Non-standard interactions can arise as a low-energy manifestation of new heavy states of a more complete model at high energy [26–30] or it can arise due to light mediators [31, 32]. NSI can modify the neutrino and antineutrino flavour conversion in matter [33–35]. Neutral current NSI during neutrino propagation can be represented by a dimension 6 operator [33]:

$$\mathcal{L}_{\text{NC-NSI}} = -2\sqrt{2}G_F\epsilon_{\alpha\beta}^{fC}(\bar{\nu}_\alpha\gamma^\mu P_L\nu_\beta)(\bar{f}\gamma_\mu P_C f), \quad (2.6)$$

where $\alpha, \beta = e, \mu, \tau$ denote the neutrino flavour, $f = e, u, d$ denotes the fermions inside matter, P is the projection operator with the superscript C referring to the L or R chirality

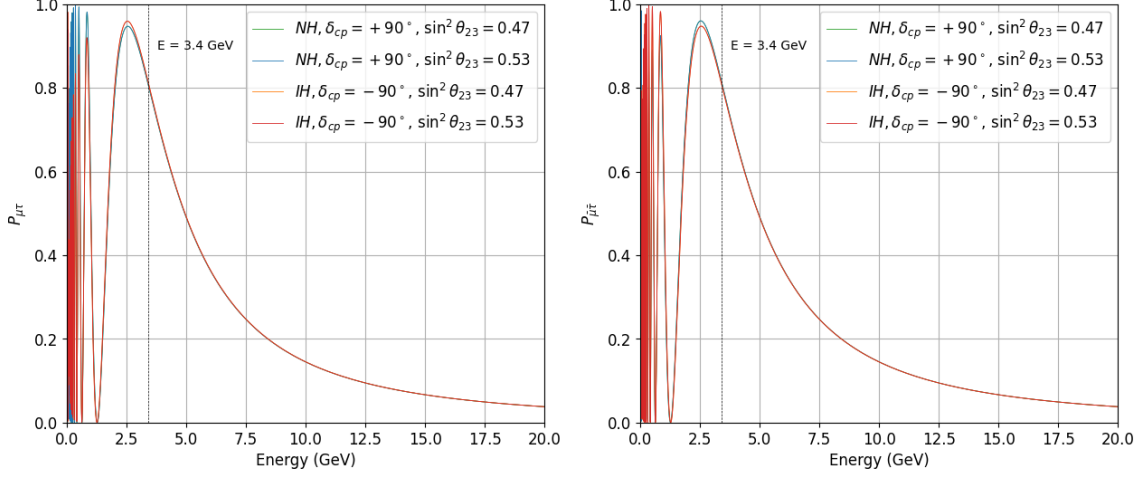


Figure 2. $\nu_{\mu} \rightarrow \nu_{\tau}$ oscillation probability as a function of energy with different $\text{NH-}\delta_{\text{CP}} = +90^\circ$ and $\text{IH-}\delta_{\text{CP}} = -90^\circ$ and θ_{23} in LO and HO for (anti-) neutrino in the (right) left panel. The hierarchy- δ_{CP} combinations, and $\sin^2 \theta_{23}$ values for different coloured lines have been mentioned on the plots. The other oscillation parameters have been fixed to the best-fit values taken from ref. [23, 24].

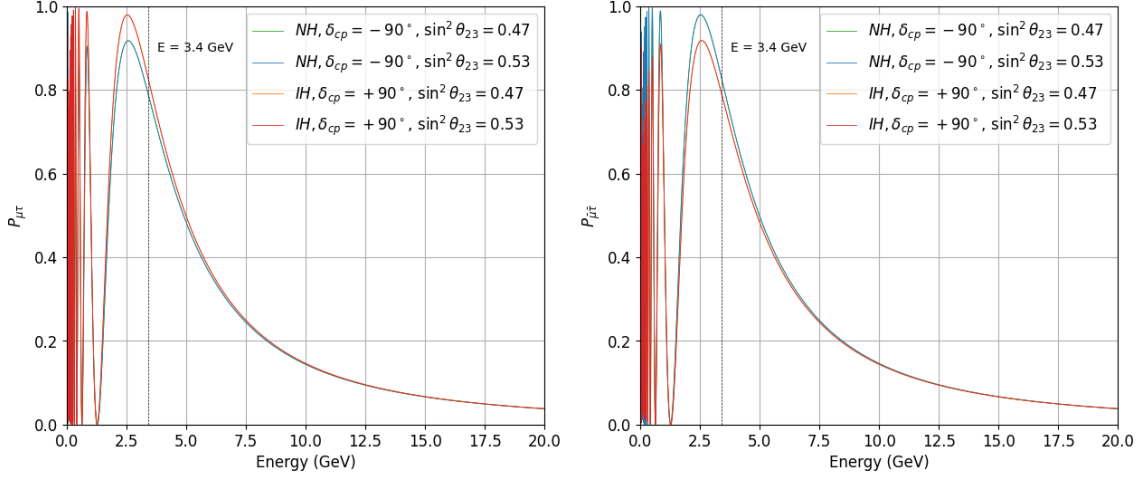


Figure 3. $\nu_{\mu} \rightarrow \nu_{\tau}$ oscillation probability as a function of energy with different $\text{NH-}\delta_{\text{CP}} = -90^\circ$ and $\text{IH-}\delta_{\text{CP}} = 90^\circ$ and θ_{23} in LO and HO for (anti-) neutrino in the (right) left panel. The hierarchy- δ_{CP} combinations, and $\sin^2 \theta_{23}$ values for different coloured lines have been mentioned on the plots. The other oscillation parameters have been fixed to the best-fit values taken from ref. [23, 24].

of the ff current, and $\epsilon_{\alpha\beta}^{fC}$ denotes the strength of the NSI. From the hermiticity of the interaction,

$$\epsilon_{\beta\alpha}^{fC} = \left(\epsilon_{\alpha\beta}^{fC} \right)^* . \quad (2.7)$$

For neutrino propagation through earth matter, the relevant expression is

$$\epsilon_{\alpha\beta} \equiv \sum_{f=e,u,d} \epsilon_{\alpha\beta}^f \frac{N_f}{N_e} \equiv \sum_{f=e,u,d} \left(\epsilon_{\alpha\beta}^{fL} + \epsilon_{\alpha\beta}^{fR} \right) \frac{N_f}{N_e}, \quad (2.8)$$

where N_f is the density of f fermion. If we consider earth matter to be neutral and isoscalar, then $N_n \simeq N_p = N_e$. Thus,

$$\epsilon_{\alpha\beta} \simeq \epsilon_{\alpha\beta}^e + 3\epsilon_{\alpha\beta}^u + 3\epsilon_{\alpha\beta}^d. \quad (2.9)$$

The effective Hamiltonian for neutrino propagation in matter in presence of NSI can be written in the flavour basis as

$$H = H_{\text{vac}} + H_{\text{mat}} + H_{\text{NSI}}, \quad (2.10)$$

where

$$H_{\text{vac}} = \frac{1}{2E} U \begin{bmatrix} m_1^2 & 0 & 0 \\ 0 & m_2^2 & 0 \\ 0 & 0 & m_3^2 \end{bmatrix} U^\dagger; H_{\text{mat}} = \sqrt{2} G_F N_e \begin{bmatrix} 1 & 0 & 0 \\ 0 & 0 & 0 \\ 0 & 0 & 0 \end{bmatrix}; \quad (2.11)$$

$$H_{\text{NSI}} = \sqrt{2} G_F N_e \begin{bmatrix} \epsilon_{ee} & \epsilon_{e\mu} & \epsilon_{e\tau} \\ \epsilon_{e\mu}^* & \epsilon_{\mu\mu} & \epsilon_{\mu\tau} \\ \epsilon_{e\tau}^* & \epsilon_{\mu\tau}^* & \epsilon_{\tau\tau} \end{bmatrix}. \quad (2.12)$$

Calculating the oscillation probabilities with NSI in a 3-flavour oscillation scheme is a non-trivial and cumbersome job. Different perturbative approaches have been taken to calculate the oscillation probabilities with NSI in references [36–38]. Following ref. [36], we can write $P_{\mu\tau}$ with NSI up to second order perturbative term as

$$P_{\mu\tau}^{\text{NSI}} = P_{\mu\tau}^{2\text{vac}} + P_{\mu\tau}^{\epsilon_{e\mu}, \epsilon_{e\tau}} + P_{\mu\tau}^{\epsilon_{\mu\mu}, \epsilon_{\mu\tau}, \epsilon_{\tau\tau}} \quad (2.13)$$

, where the leading order term is the $\nu_\mu \rightarrow \nu_\tau$ oscillation probability in vacuum with a 2-flavour scheme, and given by

$$P_{\mu\tau}^{2\text{vac}} = 4 \cos^2 \theta_{23} \sin^2 \theta_{23} \sin^2 \frac{\Delta_{31} L}{4E}. \quad (2.14)$$

As expected, the leading order term does not have dependency on hierarchy, octant or δ_{CP} . After the first term, the second term $P_{\mu\tau}^{\epsilon_{e\mu}, \epsilon_{e\tau}}$, which is a function of $\epsilon_{e\mu}$ and $\epsilon_{e\tau}$, the two NSI terms responsible for resolving the tension between NO ν A and T2K. The third term $P_{\mu\tau}^{\epsilon_{\mu\mu}, \epsilon_{\mu\tau}, \epsilon_{\tau\tau}}$ is a function of $\epsilon_{\mu\mu}$, $\epsilon_{\mu\tau}$, and $\epsilon_{\tau\tau}$. From equations B6 and B8 of ref. [36], we can see that the maximum contribution comes from $\epsilon_{\mu\tau}$, and in that case the oscillation probability becomes sensitive to hierarchy. It is because in the oscillation probability, effect of $\epsilon_{\mu\tau}$ arises in the form $\sin^2 2\theta_{23} |\epsilon_{\mu\tau}| \cos \phi_{\mu\tau} \sin(\Delta_{31} L / 2E)$. For $|\epsilon_{\mu\tau}| = 0.2$, and $\phi_{\mu\tau} = 0$, we have a hierarchy sensitive term numerically proportional to $|\epsilon_{\mu\tau}|$, making its contribution ~ 10 times larger, compared to the subleading term in eq. 2.1. However, there is no octant sensitivity for the $\epsilon_{\mu\tau}$ terms. In case of other NSI parameters, $\epsilon_{\mu\mu}$ and $\epsilon_{\tau\tau}$ terms are proportional to $\cos^2 2\theta_{23}$ making their contribution negligible, whereas $\epsilon_{e\mu}$ and $\epsilon_{e\tau}$ terms always come in second order: $|\epsilon_{e\mu}|^2$ or $|\epsilon_{e\tau}|^2$ —making their contribution negligible compared to the leading order term.

The $|\epsilon_{\mu\tau}|$ value of 0.2 is larger than the 90% limit on $|\epsilon_{\mu\tau}|$ from the IceCube data [39]. However, throughout our analysis we have chosen the true values of all the NSI

parameters to be 0.2 to compare them with the best-fit values of $|\epsilon_{e\mu}|$ and $|\epsilon_{e\tau}|$ measured by the combined analysis of NO ν A and T2K. Moreover, the latest global fit results from [40] allow NSI parameter absolute values $\sim 10^{-1}$ at a 3σ limit.

These characteristics, discussed above, have been depicted in figs. 4 and 5. In fig. 4, the first and third panels from the top represent $P_{\mu\tau}$ as a function of energy, whereas the second and fourth panels from the top represent $P_{\bar{\mu}\bar{\tau}}$ as a function of energy. We can see from this figure that the change in the $P_{\mu\tau}$ and $P_{\bar{\mu}\bar{\tau}}$ due to NSI is negligible for all NSI parameters, except $\epsilon_{\mu\tau}$. From fig. 5, we conclude that when the NSI effect is due to $\epsilon_{\mu\tau}$, it is possible to discriminate between different hierarchies at the oscillation probability level. However, it remains true that even for this case, there is no octant or δ_{CP} sensitivity. The differences between probabilities due to the change in hierarchy is very small for $\epsilon_{e\mu}$ and $\epsilon_{e\tau}$, and is even smaller for NSI due to $\epsilon_{\mu\mu}$ and $\epsilon_{\tau\tau}$. There are no differences in the probabilities due to the change in the octant of θ_{23} or δ_{CP} for these parameters.

3 Simulation details

The future long baseline accelerator neutrino oscillation experiment DUNE [41] consists of a baseline of 1300 km. It has been designed to disentangle the changes due to CP violation from the changes due to the matter effect. Its baseline and correspondingly its energy are much longer compared to NO ν A and T2K and hence the matter effect is much larger. Therefore, it is expected to measure the unknown quantities with much better precision than the ongoing accelerator neutrino long baseline experiments. For our analysis, we have used the energy resolution, energy-dependent detector efficiencies for the signal and background, and systematic uncertainties in the case of ν_μ and $\bar{\nu}_\mu$ disappearance, and ν_e and $\bar{\nu}_e$ appearance from ref.[42].

For the ν_τ and $\bar{\nu}_\tau$ appearance simulations, we have followed ref. [19]. For the energy resolution function, we have used a bin based energy smearing function

$$R^c(E, E') = \frac{1}{\sqrt{2\pi}} e^{-\frac{(E-E')^2}{2\sigma^2(E)}}, \quad (3.1)$$

where E' is the reconstructed energy. The energy resolution function is given by

$$\sigma(E) = \alpha E + \beta\sqrt{E} + \gamma. \quad (3.2)$$

As suggested in ref. [19], we have used $\alpha = 0.25$, and $\beta = \gamma = 0$. We have used the regular DUNE fluxes from ref. [42], and tau-optimized high energy flux in order to obtain a considerable number of events at energies above the τ -threshold energy, from ref. [43].

For ν_τ ($\bar{\nu}_\tau$) appearance, the signal comes from $\nu_\mu \rightarrow \nu_\tau$ ($\bar{\nu}_\mu \rightarrow \bar{\nu}_\tau$) oscillation from the ν_μ ($\bar{\nu}_\mu$) beam, and the background arises from $\bar{\nu}_\mu \rightarrow \bar{\nu}_\tau$ ($\nu_\mu \rightarrow \nu_\tau$) oscillation from the $\bar{\nu}_\mu$ (ν_μ) impurities present in the neutrino (anti-neutrino) beam as well as the intrinsic $\bar{\nu}_\tau$ (ν_τ) present in the beam, and the neutral current backgrounds. The energy dependent detector efficiencies have been calculated by matching the event numbers with the event simulations provided in ref. [19]. In ref. [19] simulations for $\bar{\nu}_\tau$ appearance, for the high energy beam, were not provided. In our analysis, we have included $\bar{\nu}_\tau$ appearance for these high energy

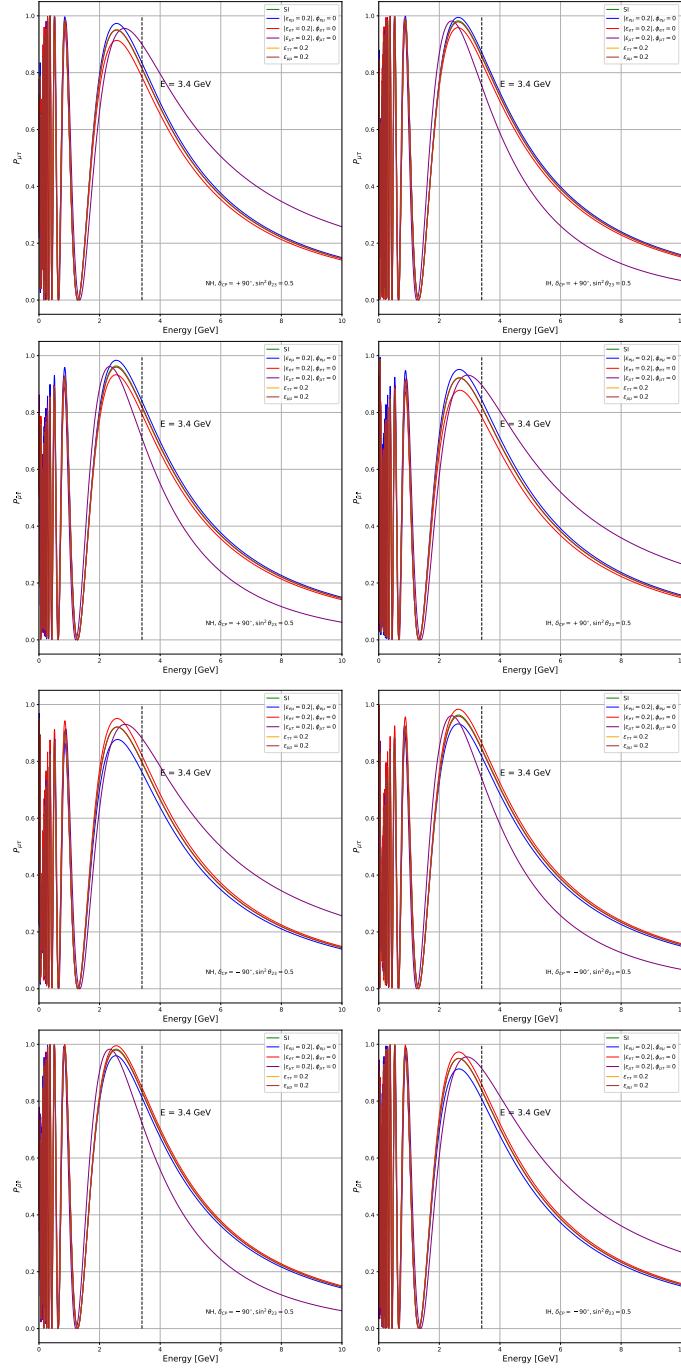


Figure 4. $\nu_\mu \rightarrow \nu_\tau$ oscillation probability for different NSI parameters as a function of energy with different NH and IH with $\delta_{CP} = 90^\circ$ and -90° , and $\sin^2 \theta_{23} = 0.5$. The δ_{CP} and $\sin^2 \theta_{23}$ values have been mentioned in the plots. The NSI parameter values for different coloured lines have been mentioned on the labels on the plots. While considering one NSI parameters, other NSI parameters have been fixed to 0. Other oscillation parameter values have been taken from ref. [23, 24].

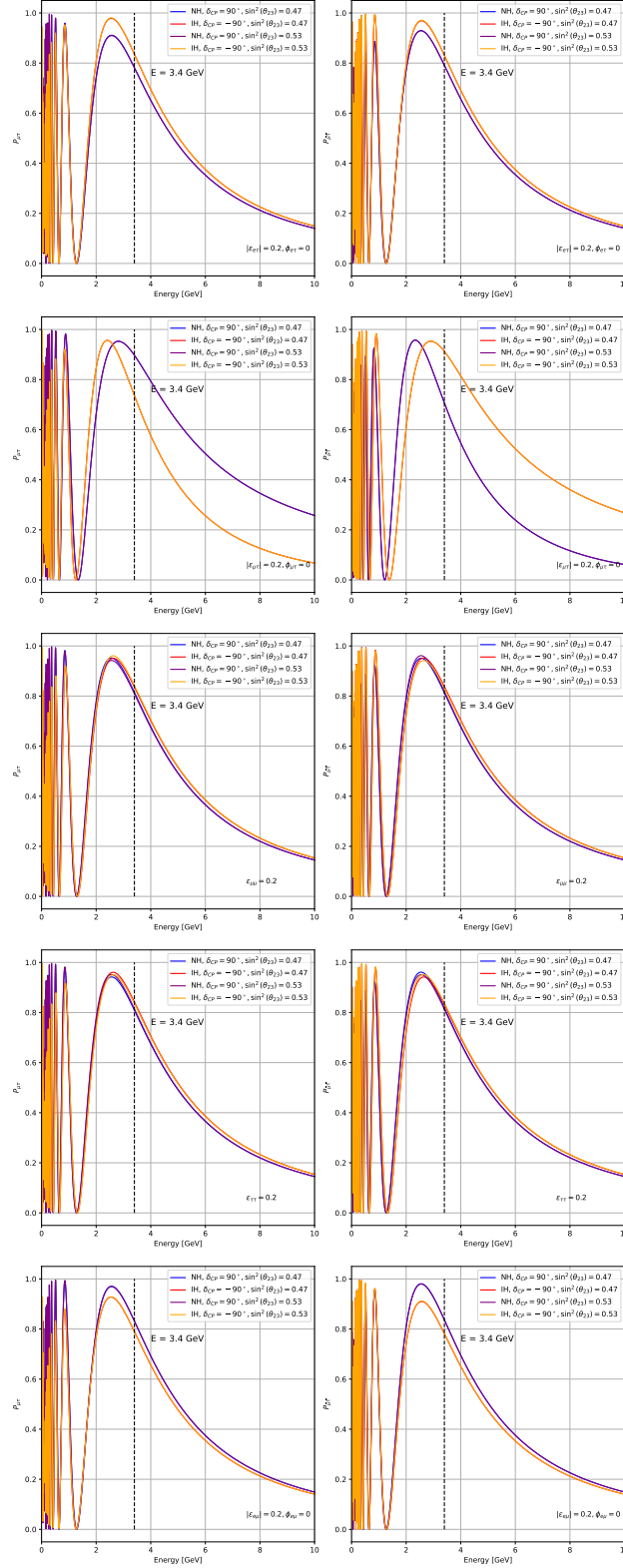


Figure 5. $\nu_\mu \rightarrow \nu_\tau$ oscillation probability for different NSI parameters as a function of energy with different hierarchies, δ_{CP} values and octant of θ_{23} . The NSI parameter values have been mentioned in the plots. The hierarchy, δ_{CP} and $\sin^2 \theta_{23}$ values for different coloured lines have been mentioned on the labels on the plots. While considering one NSI parameters, other NSI parameters have been fixed to 0. Other oscillation parameter values have been taken from ref. [23, 24].

fluxes as well. In this case, the energy dependent detector efficiencies have been calculated assuming that the ratio of signals between neutrino and anti-neutrino beams, and that of background between the neutrino and anti-neutrino beams remain the same for regular DUNE fluxes as and high energy fluxes.

For the i -th energy bin, by comparing the **true** experimental event rates, N_i^{true} , and the **test** theoretical event rates, N_i^{test} , the χ^2 has been calculated using the GLoBES software [44, 45]. The cross-section files for tau neutrino and anti-neutrino have been taken from the NO ν A experiment cross-section files provided in the GLoBES website as well. The Poissonian χ^2 between the true and test events is defined as

$$\chi^2 = 2 \sum_i \left\{ (1+z)N_i^{\text{th}} - N_i^{\text{exp}} + N_i^{\text{exp}} \ln \left[\frac{N_i^{\text{exp}}}{(1+z)N_i^{\text{th}}} \right] \right\} + 2 \sum_j (1+z)N_j^{\text{th}} + z^2 \quad (3.3)$$

where the index i represents the bins for which $N_i^{\text{exp}} \neq 0$, and j represents the bins for which $N_j^{\text{exp}} = 0$. The parameter z defines the additional systematic uncertainties. Similar systematic uncertainties as in ref. [19] have been used in this analysis. The minimum of these χ^2 values are subtracted from them to calculate $\Delta\chi^2$. For simulations, the minimum χ^2 is 0 when the true parameter values and test parameter values are equal, and hence χ^2 and $\Delta\chi^2$ are the same for simulations. In this paper, we have investigated the hierarchy sensitivity and octant sensitivity at DUNE in the presence of NSI, determination of NSI phases, and the future sensitivity to NSI parameters without and with tau-neutrino determination. The details regarding the true parameter values considered, test parameter values, and priors used to accommodate results from previous experiments are discussed in the next chapter for each of the results presented. In our analysis, we have considered five different beam running schemes, which include:

1. $5 + 5(\mu + e)$: $\nu_\mu + \bar{\nu}_\mu$ disappearance and $\nu_e + \bar{\nu}_e$ appearance after 5 years each of neutrino and anti-neutrino runs with regular DUNE fluxes.
2. $5 + 5(\mu + \tau)$: $\nu_\mu + \bar{\nu}_\mu$ disappearance and $\nu_\tau + \bar{\nu}_\tau$ appearance after 5 years each of neutrino and anti-neutrino runs with regular DUNE fluxes.
3. $5 + 5(\mu + e + \tau)$: $\nu_\mu + \bar{\nu}_\mu$ disappearance, $\nu_e + \bar{\nu}_e$ appearance and $\nu_\tau + \bar{\nu}_\tau$ appearance after 5 years each of neutrino and anti-neutrino runs with regular DUNE fluxes.
4. $5 + 5 + 1 + 1(\mu + \tau)$: $\nu_\mu + \bar{\nu}_\mu$ disappearance and $\nu_\tau + \bar{\nu}_\tau$ appearance after 5 years each of neutrino and anti-neutrino runs with regular DUNE fluxes, along with $\nu_\mu + \bar{\nu}_\mu$ disappearance and $\nu_\tau + \bar{\nu}_\tau$ appearance from 1 additional year each of neutrino and anti-neutrino running with the high energy fluxes.
5. $5 + 5 + 1 + 1(\mu + e + \tau)$: $\nu_\mu + \bar{\nu}_\mu$ disappearance, $\nu_e + \bar{\nu}_e$ appearance and $\nu_\tau + \bar{\nu}_\tau$ appearance after 5 years each of neutrino and anti-neutrino runs with regular DUNE fluxes, along with $\nu_\mu + \bar{\nu}_\mu$ disappearance and $\nu_\tau + \bar{\nu}_\tau$ appearance from 1 additional year each of neutrino and anti-neutrino running with the high energy fluxes.

For all of the cases considered, the number of protons on target is 1.1×10^{21} per year for both the regular DUNE flux and high energy τ optimized flux.

4 Results and discussions

The bi-event plots for different NSI parameters are presented in figs. 6-8. In each case, by varying δ_{CP} , the plot takes an elliptical shape. We have considered ν and $\bar{\nu}$ runs for 5 years each with regular DUNE fluxes as well as 1 year each with high energy DUNE fluxes. Fig. 6 shows that the ellipses for different NSI parameters overlap with each other and with the ellipse due to the standard oscillation case. The only exception is when the NSI due to the $\epsilon_{\mu\tau}$ parameter. There are no overlaps between the ellipse due to $\epsilon_{\mu\tau}$ and any of the other ellipses. Hence, it can be concluded that there will be no large discrimination sensitivity to different NSI parameters, except $\epsilon_{\mu\tau}$ from the ν_τ and $\bar{\nu}_\tau$ appearance channels.

In fig. 7, we show the bi-event plots for ν_e and $\bar{\nu}_e$ appearance after neutrino and anti-neutrino runs of 5 years each with regular DUNE fluxes. It can be seen that for NSI with $\epsilon_{e\mu}$ and $\epsilon_{e\tau}$, there are very small overlaps with the standard oscillation case, leading to good sensitivity to these parameters from the ν_e and $\bar{\nu}_e$ appearance channels. However, the ellipses due to these two NSI parameters have large overlaps with each other, making it difficult to differentiate between them. The separations between different δ_{CP} values on these ellipses are large, and hence we can expect good CP violation sensitivity from the ν_e and $\bar{\nu}_e$ appearance channels for NSI due to $\epsilon_{e\mu}$ and $\epsilon_{e\tau}$. For all the NSI parameters, the ellipses overlap with the ellipse due to standard oscillation. Hence, we should not expect any sensitivity to these parameters from the ν_e and $\bar{\nu}_e$ appearance channels. From fig. 8, we can see that for the standard oscillation scenario, after ν and $\bar{\nu}$ runs of 5 years each with regular DUNE fluxes, the ellipses due to different hierarchies are far apart from each other. The small differences between the two hierarchies at the probability level, manifests into a considerable difference in event numbers due to the large DUNE fluxes. However, for a particular hierarchy, the ellipses for different θ_{23} octants overlap on each other, leading to no octant sensitivity from the ν_τ and $\bar{\nu}_\tau$ appearance channels for the standard oscillation. These characteristics remain unchanged for NSI due to different parameters as well. It is to be noted that the differences between event numbers for NH and IH is not more than 1σ , except for $\epsilon_{\mu\tau}$. Therefore, apart from NSI due to $\epsilon_{\mu\tau}$, we should not expect more than 1σ hierarchy sensitivity from the ν_τ and $\bar{\nu}_\tau$ appearance channels in DUNE.

In fig. 9, we show the bi-event plots, similar to fig. 6 with regular DUNE fluxes, but for higher order values of NSI parameters. It is evident that the effect of NSI parameters $\epsilon_{e\mu}$, $\epsilon_{e\tau}$, $\epsilon_{\mu\mu}$ and $\epsilon_{\tau\tau}$ on τ neutrino and anti-neutrino appearances can be separated from that of standard interaction only when the absolute values of the individual parameters are larger than 1. These large values of NSI parameters are ruled out at 3σ level by the present global fit [40]. Therefore, it is evident that the visible effects from NSI parameters $\epsilon_{e\mu}$, $\epsilon_{e\tau}$, $\epsilon_{\mu\mu}$ and $\epsilon_{\tau\tau}$ on ν_τ and $\bar{\nu}_\tau$ appearances can only occur from unphysical values of these NSI parameters.

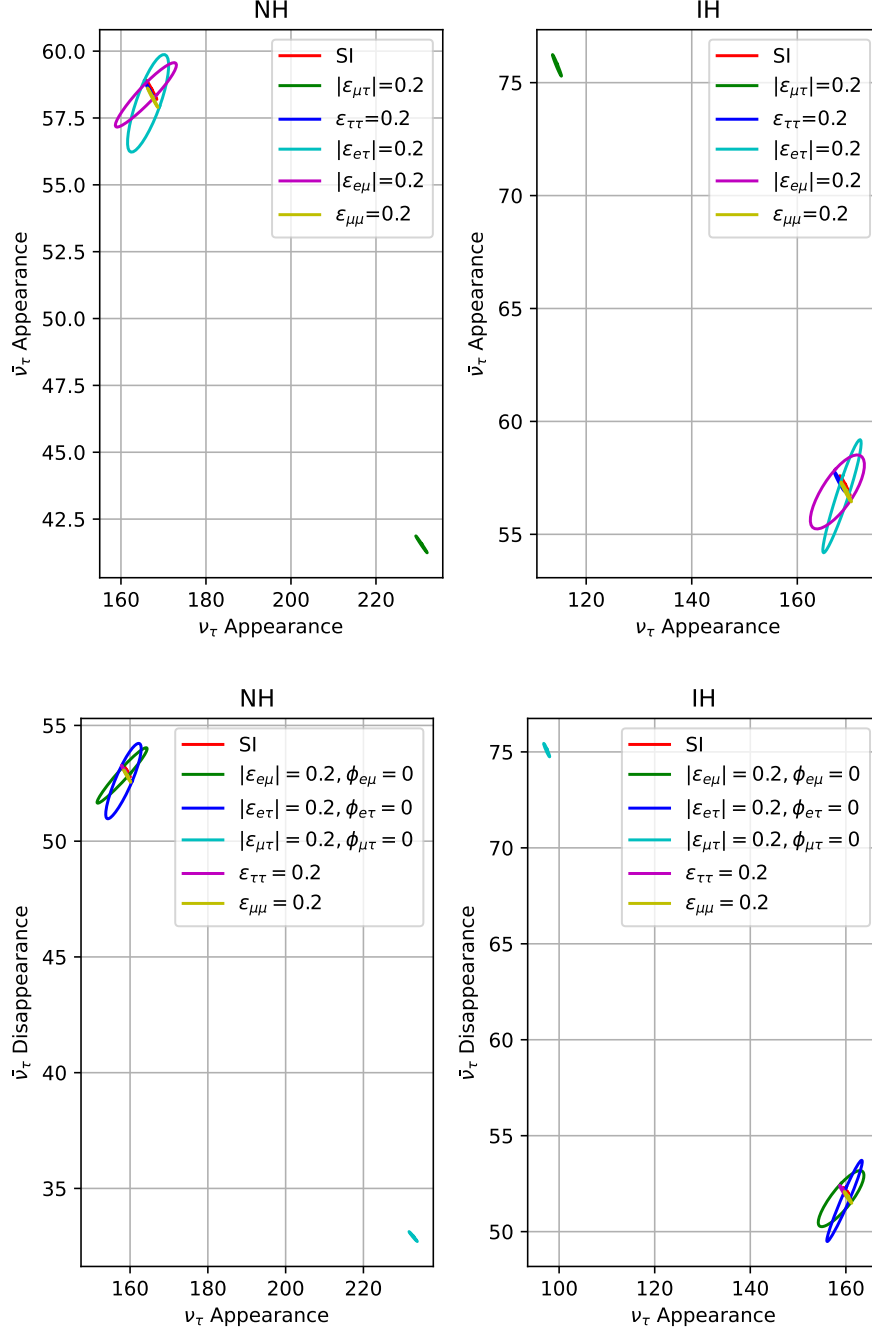


Figure 6. $\bar{\nu}_\tau$ vs ν_τ event numbers after varying δ_{CP} in the range $[-180^\circ : 180^\circ]$ for NH (IH) in the left (right) panel after 5 years (1 year) each of neutrino and anti-neutrino run with regular (τ optimized high energy) DUNE fluxes in the top (bottom) panel. All the other standard oscillation parameter values have been taken from ref. [23, 24]. Different NSI parameter values have been mentioned on the figure.

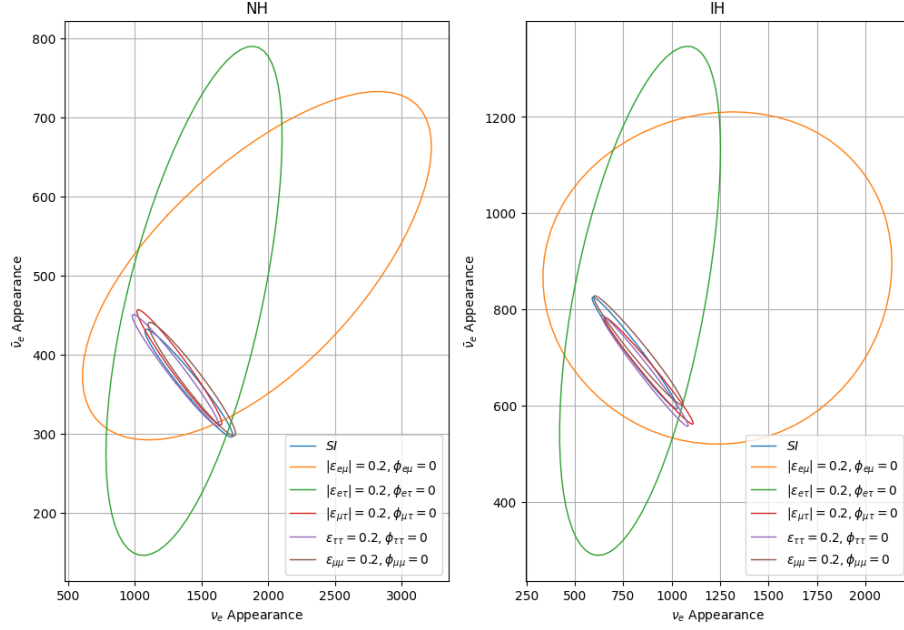


Figure 7. $\bar{\nu}_e$ vs ν_e event numbers after varying δ_{CP} in the range $[-180^\circ : 180^\circ]$ for NH (IH) in the left (right) panel after 5 years each of neutrino and anti-neutrino run with regular DUNE fluxes. All the other standard oscillation parameter values have been taken from ref. [23, 24]. Different NSI parameter values have been mentioned on the figure.

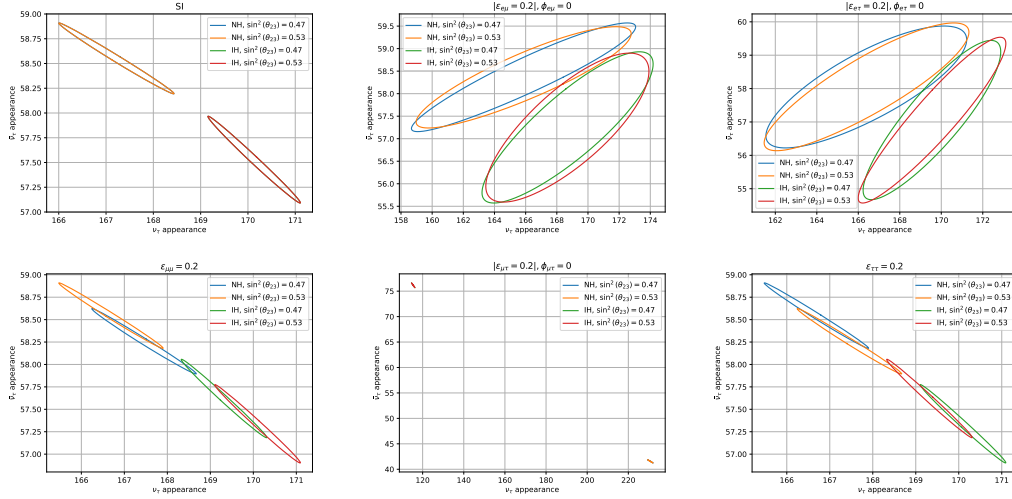


Figure 8. $\bar{\nu}_\tau$ vs ν_τ event numbers after varying δ_{CP} in the range $[-180^\circ : 180^\circ]$ for different NSI parameters with different hierarchy-octant combinations as mentioned in the panels, after 5 years each of neutrino and anti-neutrino run with regular DUNE fluxes. All the other standard oscillation parameter values have been taken from ref. [23, 24]. Different NSI parameter values have been mentioned on the figure.

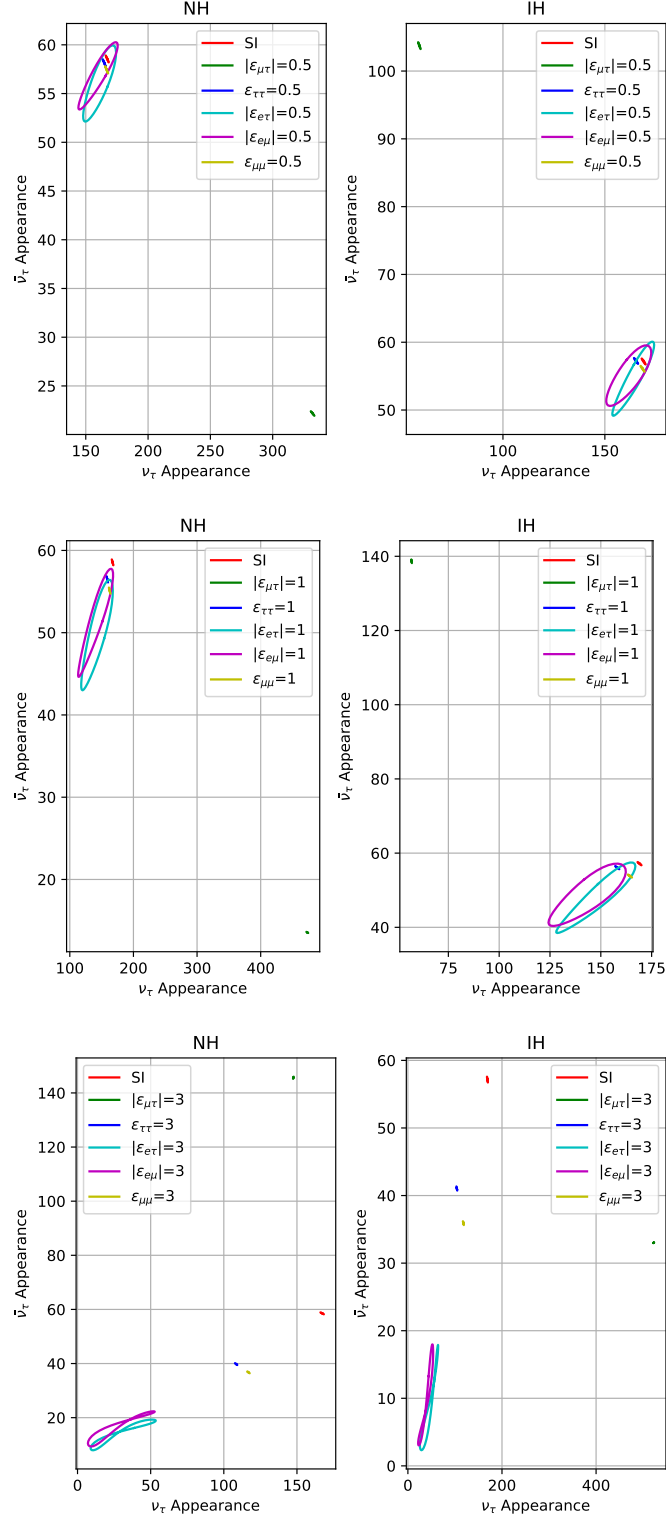


Figure 9. $\bar{\nu}_\tau$ vs ν_τ event numbers after varying δ_{CP} in the range $[-180^\circ : 180^\circ]$ for NH (IH) in the left (right) panel after 5 years each of neutrino and anti-neutrino run with regular DUNE fluxes, and for different values of NSI parameters. All the other standard oscillation parameter values have been taken from ref. [23, 24]. Different NSI parameter values have been mentioned on the figure.

4.1 Mass hierarchy sensitivity

The first test involves the investigation of DUNE's sensitivity to the mass hierarchy with and without τ neutrino detection in the absence of NSI. To perform the test, we kept both the true and test values of the NSI parameters fixed to 0. The true values of δ_{CP} have been varied in the range $[-180^\circ : 180^\circ]$. The true values of other standard oscillation parameters have been fixed to their best-fit values taken from ref. [23]. For the test values, we have varied $\sin^2 \theta_{23}$ and $|\Delta_{31}|$ in their 3σ range taken from ref. [23]. The test values of δ_{CP} have been varied in their complete range. After calculating $\Delta\chi^2$ between the true and test event numbers, marginalisation has been performed over all of the test parameters and the result is shown in fig. 10. This figure shows that for standard oscillation, the detection of τ neutrinos does not have any effect on the determination of the mass hierarchy at DUNE. The $5 + 5(\mu + e)$ run alone can determine the mass hierarchy at more than 20σ when NH (IH) and $\delta_{\text{CP}} = -90^\circ$ ($+90^\circ$) are the true hierarchy- δ_{CP} combination, and close to (more than) 10σ when NH (IH) and $\delta_{\text{CP}} = +90^\circ$ (-90°) are the true hierarchy- δ_{CP} combination. This sensitivity does not change with the addition of ν_τ and $\bar{\nu}_\tau$ channels. In

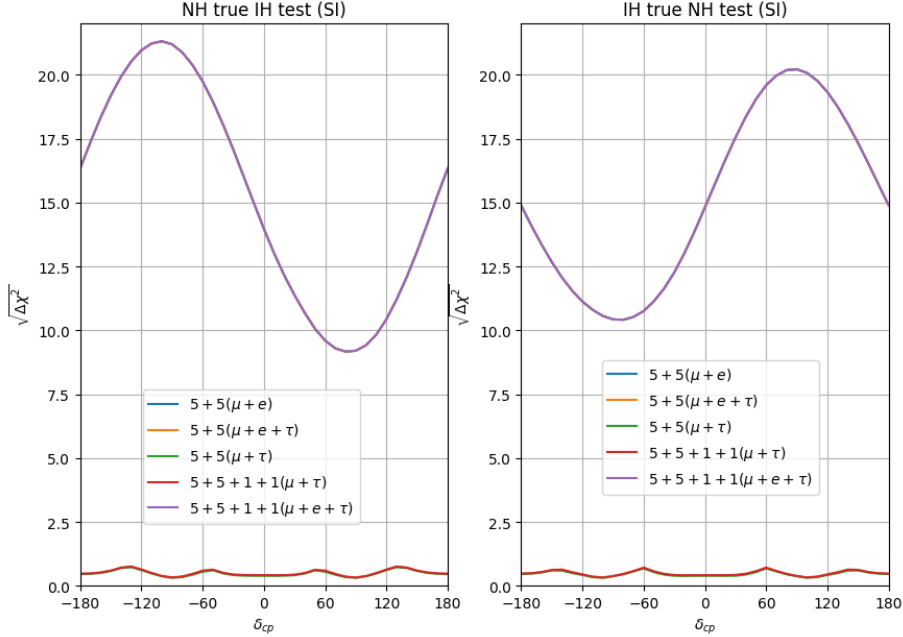


Figure 10. Hierarchy sensitivity of DUNE without the presence of any NSI and for different running schemes. The left (right) panel is for the true hierarchy being NH (IH).

the next step, we have considered NSI with one parameter at a time. The true value of the NSI parameter has been fixed to 0.2 with the true value of the corresponding phase, when necessary, fixed at 0. We have already stated in section 2, that for $\epsilon_{\mu\mu}$ and $\epsilon_{\mu\tau}$, these values are outside the 90% limit given by IceCube [39]. Still we choose these values to be consistent with the best-fit values of $\epsilon_{e\mu}$ and $\epsilon_{e\tau}$ from the combined analysis of NO ν A and T2K, and because $\sim 10^{-1}$ values for $\epsilon_{\mu\mu}$ and $|\epsilon_{\mu\tau}|$ are allowed at 3σ level by the global fits of ref. [40]. The test values of the NSI parameters have been varied in the range

[0 : 3] for the absolute values of the non-diagonal parameters $\epsilon_{e\mu}$, $\epsilon_{e\tau}$ and $\epsilon_{\mu\tau}$, with their phases varied in the range $[-180^\circ : 180^\circ]$. In case of diagonal parameters $\epsilon_{\mu\mu}$ and $\epsilon_{\tau\tau}$, the test values have been varied in the range $[-3 : 3]$. The marginalisation of $\Delta\chi^2$ has been performed over both the standard and NSI test parameters. The results are shown in fig. 11. It can be seen that the ν_τ and $\bar{\nu}_\tau$ appearance channels do not improve the hierarchy sensitivity when compared to the ν_e and $\bar{\nu}_e$ appearance channels. The inclusion of NSI reduces the hierarchy sensitivity for the $5 + 5(\mu + e)$ run for the case of $\epsilon_{e\mu}$, and more significantly for the case of $\epsilon_{e\tau}$. The fluctuations we see in these two cases, are due to the interference between δ_{CP} and the phases $\phi_{e\mu}$ and $\phi_{e\tau}$. In case of NSI due to $\epsilon_{\mu\tau}$, we do not see these fluctuations because the interference term between δ_{CP} and $\phi_{\mu\tau}$ do not exist in the expression of $P_{\mu e}$ and $P_{\bar{\mu}e}$. Similarly, the fluctuations in the case of $\epsilon_{\mu\mu}$ and $\epsilon_{\tau\tau}$ are missing because of the absence of phases in these two real terms. The low hierarchy sensitivity in the ν_τ and $\bar{\nu}_\tau$ appearance channels in case of NSI due to $\epsilon_{\mu\tau}$ is counter intuitive because we can see large separation in the bi-event plots for NH and IH from fig. 8 and also from the probability plots in fig. 5. However, the hierarchy sensitivity for $\epsilon_{\mu\tau}$ comes from the $\sin^2 2\theta_{23} |\epsilon_{\mu\tau}| \cos \phi_{\mu\tau} \sin(\Delta_{31} L/2E)$ term in $P_{\mu\tau}$ and $P_{\bar{\mu}\tau}$, as discussed in section 2. Therefore, the $P_{\mu\tau}$ and $P_{\bar{\mu}\tau}$ for NH at $|\epsilon_{\mu\tau}| = 0.2$, and $\phi_{\mu\tau} = 0$, can be mimicked by choosing IH, $|\epsilon_{\mu\tau}| = 0.2$, and $\phi_{\mu\tau} = 180^\circ$. Similarly, the $P_{\mu\tau}$ and $P_{\bar{\mu}\tau}$ for IH at $|\epsilon_{\mu\tau}| = 0.2$ and $\phi_{\mu\tau} = 0$, can be mimicked by choosing NH, $|\epsilon_{\mu\tau}| = 0.2$, and $\phi_{\mu\tau} = 180^\circ$. Similarly, for any true hierarchy and true value of $\phi_{\mu\tau}$, the hierarchy sensitivity can be cancelled by choosing a test $\phi_{\mu\tau}$ as $\phi_{\mu\tau}(\text{test}) = 180^\circ - \phi_{\mu\tau}(\text{true})$. Therefore, a new degeneracy in form of $\phi_{\mu\tau}$ -hierarchy arises due to the $\cos \phi_{\mu\tau}$ dependency of the hierarchy sensitive part of the oscillation probability expression. Since we are marginalizing over $\phi_{\mu\tau}$, this degeneracy effectively reduces the hierarchy sensitivity in the τ appearance channels even in the case of $\epsilon_{\mu\tau}$. We have emphasized this argument in fig. 12. The figure shows that the hierarchy sensitivity for NSI due to $\epsilon_{\mu\tau}$ is lost due to the $\phi_{\mu\tau}$ -hierarchy degeneracy.

4.2 CP violation sensitivity

In this section, we present the potential of DUNE to reject CP conserving δ_{CP} values, and how the detection of ν_τ can affect the sensitivity for different running schemes.

Firstly, we consider the standard 3-flavour oscillation without the presence of any NSI. For this case, we have fixed the true values of the standard oscillation parameters, except δ_{CP} , at the global best-fit values of ref. [23]. The true values of δ_{CP} have been varied in the range $[-180^\circ : 180^\circ]$. For the test values of oscillation parameters, we have varied $\sin^2 \theta_{23}$ and $|\Delta_{31}|$ in their 3σ range given in ref. [23]. The test values of δ_{CP} are the three CP conserving values, namely 0, -180° and 180° . Both the hierarchies have been considered as the test hierarchy. The χ^2 between true and test events numbers have been calculated. In this case also, χ^2 and $\Delta\chi^2$ are basically same. The marginalisation of $\Delta\chi^2$ has been performed over the test parameter values, and the final result is presented using $\Delta\chi^2$ as a function of the true δ_{CP} , as shown in fig. 13. The figure shows that when NH is the true hierarchy, the maximum CP violation sensitivity can be established at $> 6\sigma$ and $> 7.5\sigma$ for $\delta_{\text{CP}} \sim -50^\circ$ and $\delta_{\text{CP}} \sim 150^\circ$ respectively in the case of $5 + 5(\mu + e)$ run. For the same run, when IH is the true hierarchy, CP sensitivity of maximum 7σ can be

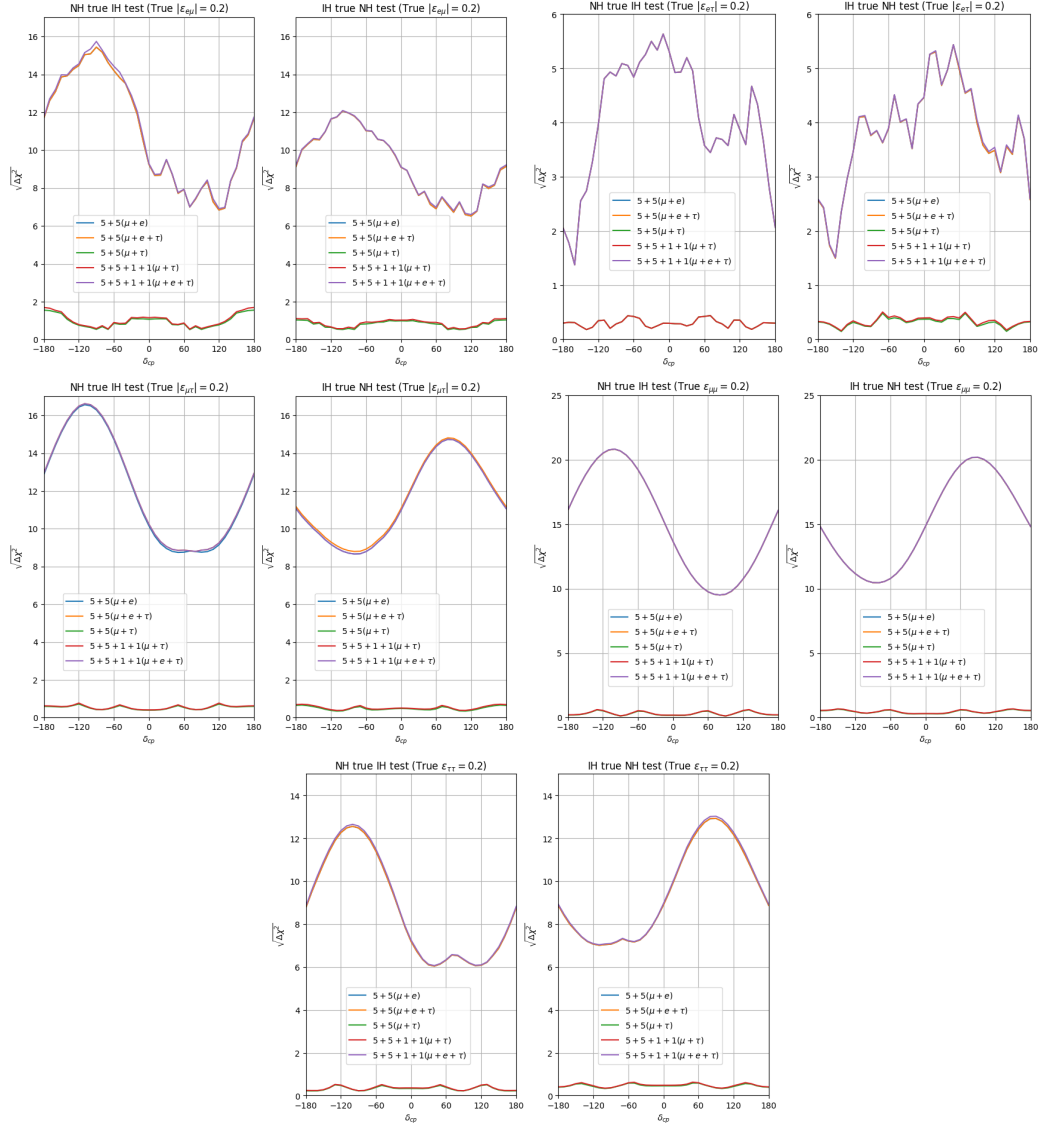


Figure 11. Hierarchy sensitivity of DUNE with the presence of NSI and for different running schemes. The left (right) panel is for the true hierarchy being NH (IH). The true values of NSI parameters have been mentioned on top of the each plot.

established at $\delta_{CP} = \pm 100^\circ$. Addition of ν_τ and $\bar{\nu}_\tau$ will not have any significant changes to the CP violation sensitivity of DUNE. Only 1σ discovery of CP violation is possible with $5 + 5(\mu + \tau)$ and $5 + 5 + 1 + 1(\mu + \tau)$ run in case of $\delta_{CP} = \pm 100^\circ$ for both the hierarchies.

In the next step, we have considered NSI due to $\epsilon_{e\mu}$. The true values of $|\epsilon_{e\mu}|$ and $\phi_{e\mu}$ have been taken to be 0.2 and 0 respectively. The test values of $|\epsilon_{e\mu}|$ have been varied in the range $[0 : 3]$, whereas the test values of $\phi_{e\mu}$ have been varied in the range $[-180^\circ : 180^\circ]$. The true and test values of standard parameters are the same as in the previous section. As in the previous case, the marginalisation of the $\Delta\chi^2$ has been performed over the test parameter values. A similar procedure has been repeated for $\epsilon_{e\tau}$ and $\epsilon_{\mu\tau}$ as well. For the

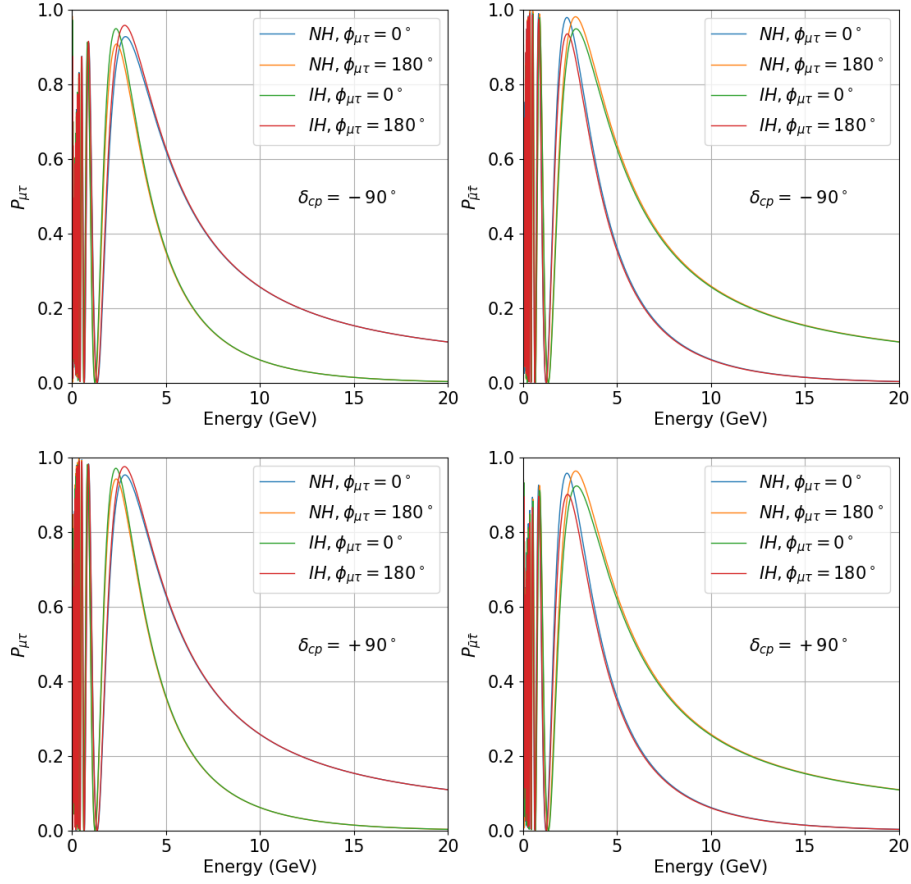


Figure 12. $P_{\mu\tau}$ ($P_{\bar{\mu}\bar{\tau}}$) in the left (right) panel as a function of neutrino energy for both the hierarchies and $\phi_{\mu\tau}$ being 0 and 180° . The δ_{CP} value is -90° (90°) in the top (bottom) panel.

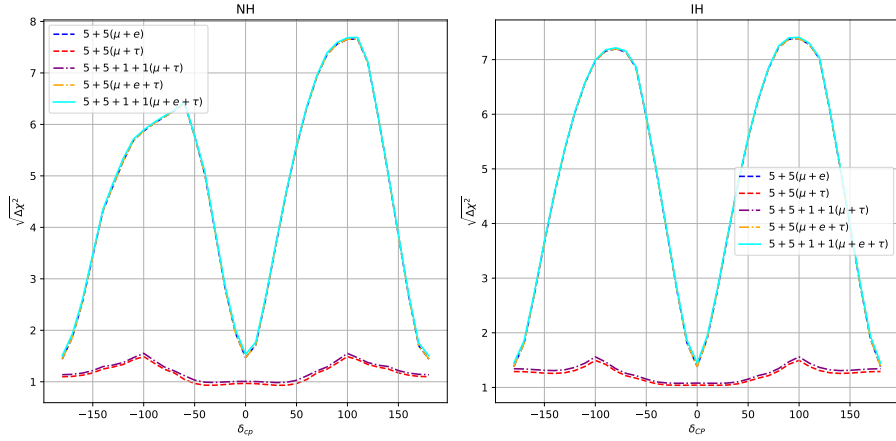


Figure 13. CP sensitivity of DUNE without the presence of any NSI and for different running schemes. The left (right) panel is for the true hierarchy being NH (IH).

case of $\epsilon_{\mu\mu}$ and $\epsilon_{\tau\tau}$, no phase has been considered and the test values of these two parameters have been varied in the range $[-3 : 3]$. The results have been shown in fig. 14. It is clear that just like in the case without NSI, with NSI the $5 + 5(\mu + \tau)$ and $5 + 5 + 1 + 1(\mu + \tau)$ running schemes have negligible sensitivity to CP violation.

4.3 Octant sensitivity

In this section, we discuss the sensitivity to determine the octant of θ_{23} . At first, we have considered the standard unitary 3×3 mixing, without the presence of any NSI. To do so, we have fixed the true values of the standard parameters at the global best-fit values taken from ref. [23]. For test parameters, we have varied δ_{CP} in the whole range of $[-180^\circ : 180^\circ]$. We also varied $\sin^2 \theta_{23}$ and $|\Delta_{31}|$ in their 3σ range. Marginalisation of $\Delta\chi^2$ has been done over $|\Delta_{31}|$ and the result has been presented as a contour plot on the test $\delta_{\text{CP}} - \sin^2 \theta_{23}$ plane. As can be seen from fig. 15, a $5 + 5(\mu + e)$ run can rule out the wrong octant for both cases of true hierarchy. However, the $5 + 5(\mu + \tau)$ and $5 + 5 + 1 + 1(\mu + \tau)$ running scenarios do not have any octant sensitivity. This is expected from our discussions in section 2.

In the next step, we considered one NSI parameter at a time. We assumed the true value of the respective NSI parameter to be 0.2. In case of non-diagonal NSI parameters, the true value of the phase associated with the NSI parameter have been considered to be 0. The test value of the concerned NSI parameter has been varied in the range $[0 : 3]$. For the non-diagonal NSI parameters, the corresponding phases have been varied in the range $[-180^\circ : 180^\circ]$. The marginalisation of $\Delta\chi^2$ has been done over test values of $|\Delta_{31}|$ and the NSI parameter and its corresponding phase when applicable. As expected from the bi-event plots, $5 + 5(\mu + \tau)$ and $5 + 5 + 1 + 1(\mu + \tau)$ runs do not have any octant sensitivity in presence of NSI. However, there is also no octant sensitivity for the $5 + 5(\mu + e)$ run, in presence of NSI due to $\epsilon_{e\mu}$ and $\epsilon_{e\tau}$, and for IH being the true hierarchy. The results for $\epsilon_{e\mu}$ and $\epsilon_{e\tau}$ are presented in fig. 16. The results for other NSI parameters have been shown in the appendix B

4.4 Determining NSI phases

In section 4.1, we have seen that the hierarchy sensitivity of the ν_τ appearance channels at DUNE in the presence of NSI due to $\epsilon_{\mu\tau}$ is reduced due to the $\phi_{\mu\tau}$ -hierarchy degeneracy arising from the $\cos \phi_{\mu\tau}$ term present in the hierarchy sensitive term of $P_{\mu\tau}$. However, due to the presence of the same term, it is possible to measure $\phi_{\mu\tau}$ with ν_τ appearance at DUNE in presence of NSI due to $\epsilon_{\mu\tau}$, when the hierarchy is measured with precision from the electron appearance channels of DUNE. The validity of this statement can be verified from fig. 12 as well. In this section, we investigate the potential of DUNE to measure NSI phases in case NSI is present in nature. To do that, we have fixed the true values of the standard oscillation parameters at their best-fit values. The true values of $|\epsilon_{e\mu}|$, $\epsilon_{e\tau}$ and $\epsilon_{\mu\tau}$ (only one at a time) have been fixed to 0.2, and the corresponding phase has been fixed to 0. The test values of δ_{CP} have been varied in the range $[-180^\circ : 180^\circ]$. The test values of $|\Delta_{31}|$, and $\sin \theta_{23}$ have been varied in their 3σ allowed values. The test values of the magnitude of the corresponding NSI parameter have been varied in the range $[0 : 3]$. Test values of the corresponding phases have been varied in the range $[-180^\circ : 180^\circ]$. The true

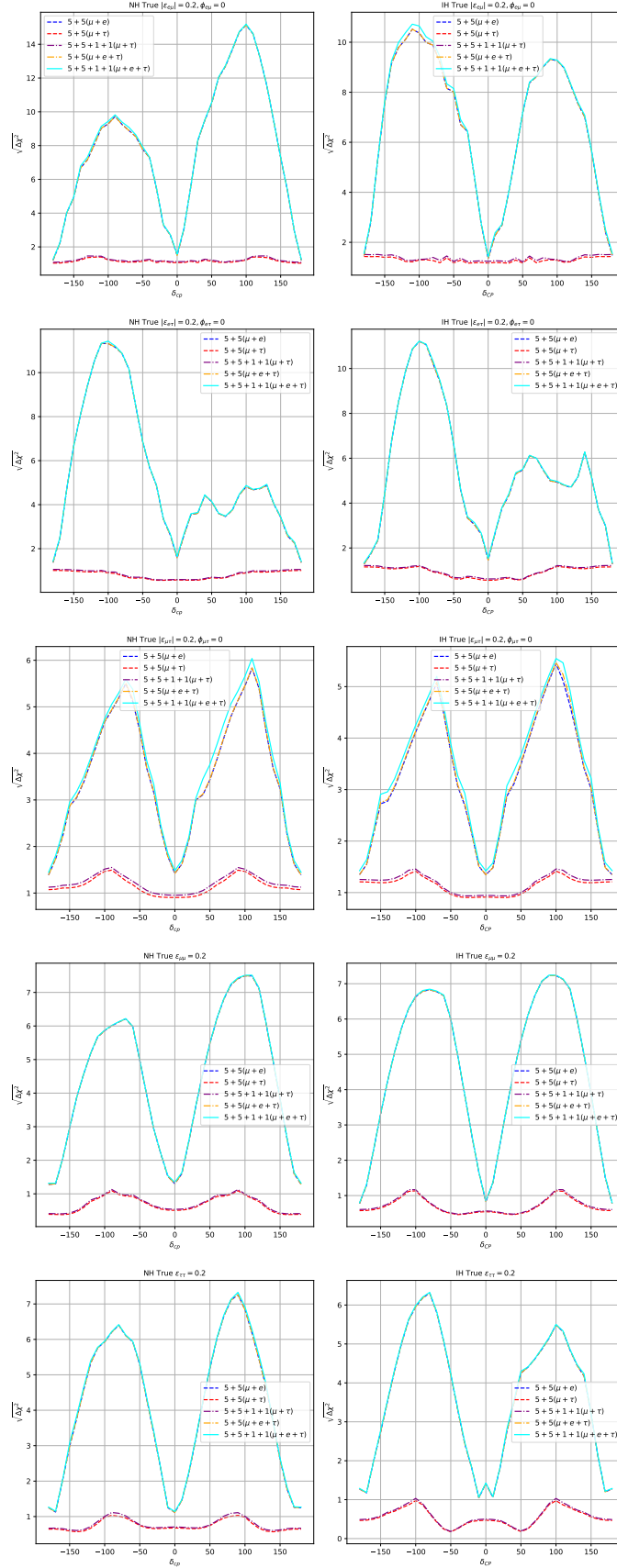


Figure 14. CP sensitivity of DUNE with the presence of NSI and for different running schemes. The left (right) panel is for the true hierarchy being NH (IH). The true values of NSI parameters have been mentioned on top of the each plot.

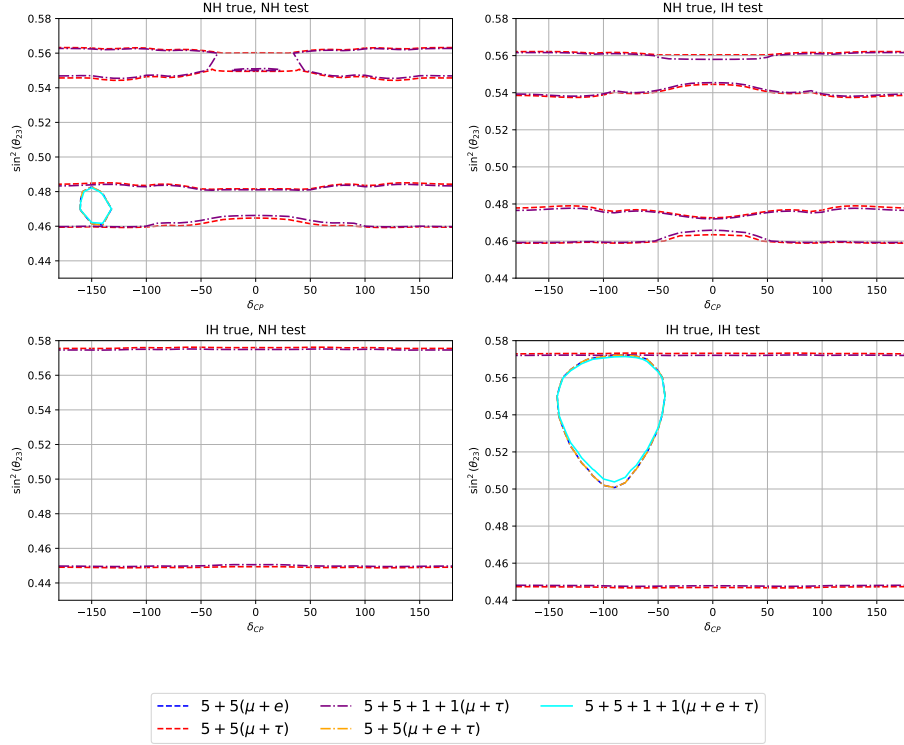


Figure 15. Allowed regions in the test $\delta_{CP} - \sin^2\theta_{23}$ plane for standard oscillation without any NSI. The top (bottom) panels are for NH (IH) being the true hierarchy. The left (right) panels are for test hierarchy being NH (IH).

and test hierarchies are the same. We have marginalised the $\Delta\chi^2$ between true and test event numbers over all the test parameters except the relevant NSI phase and the results are presented in fig. 17. The goal of the investigation is to determine, if NSI is present and the NSI phase value chosen by nature is 0, how well do the different running schemes of DUNE rule out non-zero values of the phase provided the mass hierarchy is already known with precision. In case of NSI due to $\epsilon_{e\mu}$, $40^\circ < \phi_{e\mu} < -40^\circ$ ($10^\circ < \phi_{e\mu} < -60^\circ$) can be ruled out at 5σ with only the $5 + 5(\mu + e)$ run when NH (IH) is the true hierarchy. The addition of ν_τ and $\bar{\nu}_\tau$ appearance channels does not improve the sensitivity. The $5 + 5(\mu + \tau)$ and $5 + 5 + 1 + 1(\mu + \tau)$ runs rule out $\phi_{e\mu} = \pm 90^\circ$ at 2σ confidence level for NH being the true hierarchy. This sensitivity arises from the muon disappearance channels. In case of NSI due to $\epsilon_{e\tau}$, with $5 + 5(\mu + e)$ run, $30^\circ < \phi_{e\tau} < -30^\circ$ can be ruled out at more than 5σ for both the hierarchies. The addition of ν_τ and $\bar{\nu}_\tau$ appearance data does not improve the sensitivity. In case of NSI due to $\epsilon_{\mu\tau}$, we can see that the $5 + 5(\mu + e)$, $5 + 5(\mu + \tau)$ and $5 + 5 + 1 + 1(\mu + \tau)$ runs can rule out $60^\circ < \phi_{\mu\tau} < -60^\circ$ at 5σ C.L. However, for ruling out $90^\circ < \phi_{\mu\tau} < -90^\circ$, $5 + 5 + 1 + 1(\mu + \tau)$ and $5 + 5 + 1 + 1(\mu + e + \tau)$ runs can improve the sensitivity by 1σ and 2.5σ respectively compared to the sensitivity for the $5 + 5(\mu + e)$ run, when NH is the true mass hierarchy. In case of IH being the true mass hierarchy, this improvement is 2.5σ for both the $5 + 5 + 1 + 1(\mu + \tau)$ and $5 + 5 + 1 + 1(\mu + e + \tau)$ runs. Hence, the determination of ν_τ and $\bar{\nu}_\tau$ appearance can improve the precision of $\phi_{\mu\tau}$ in case

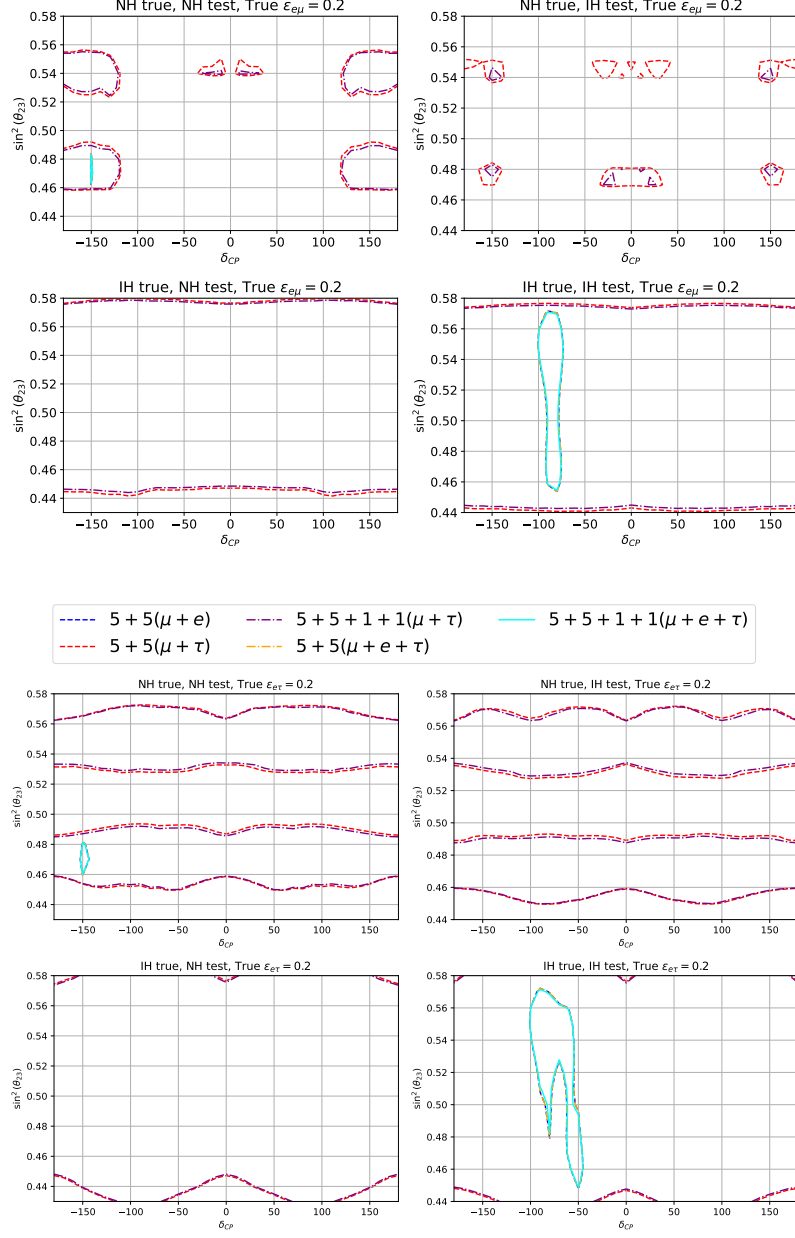


Figure 16. Allowed regions in the test $\delta_{CP} - \sin^2\theta_{23}$ plane for oscillation with NSI due to $\epsilon_{e\mu}$ and $\epsilon_{e\tau}$. The top (bottom) panels are for NH (IH) being the true hierarchy. The left (right) panels are for test hierarchy being NH (IH).

of NSI due to $\epsilon_{\mu\tau}$, given that $|\epsilon_{\mu\tau}| \sim 10^{-1}$ and the mass hierarchy is precisely known.

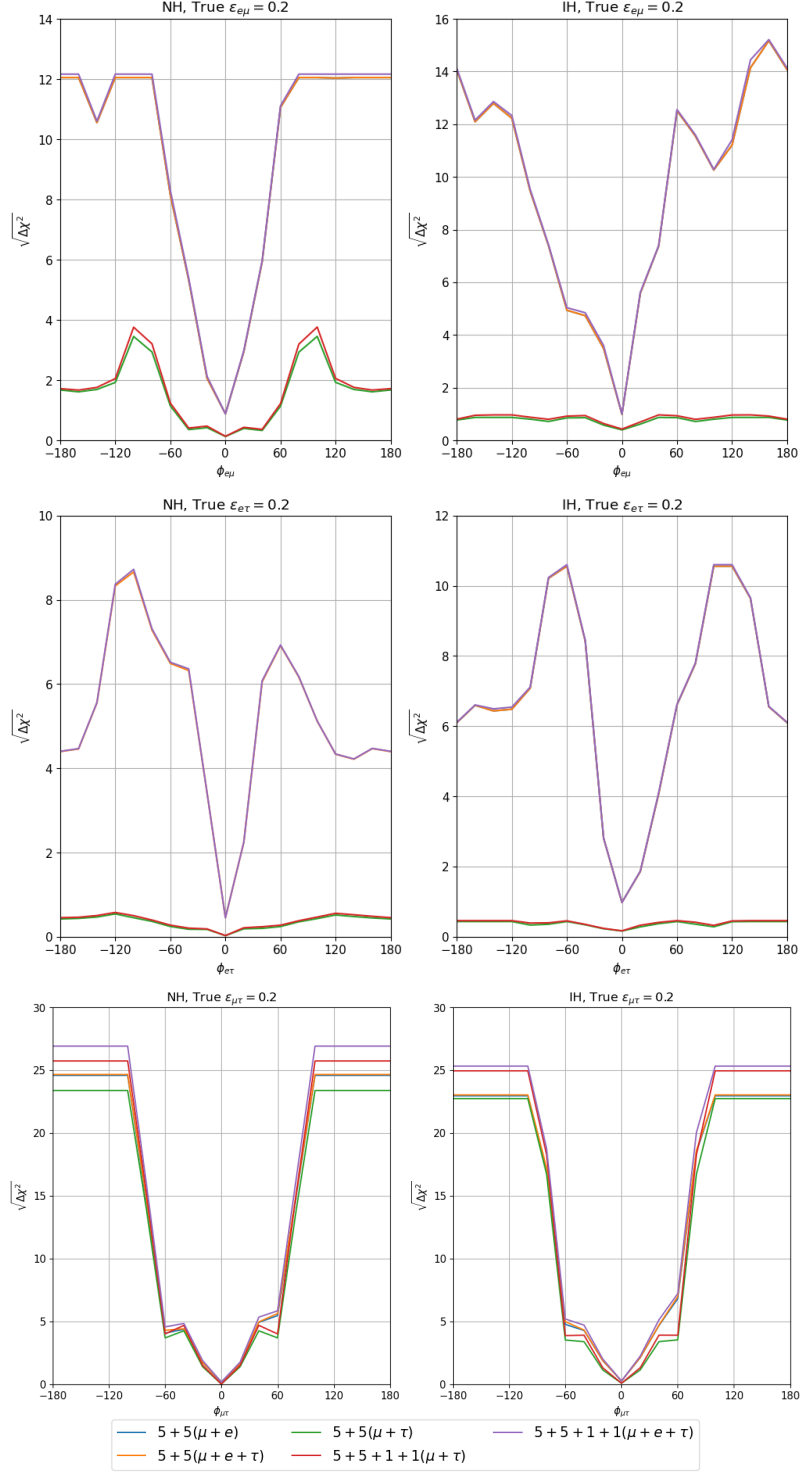


Figure 17. Determination sensitivity to different NSI phases with different runtimes of DUNE.

4.5 Sensitivity to NSI parameters

In this section, we investigate the sensitivities of different NSI parameters at DUNE and the effect of τ neutrino detection on the sensitivity. The true event rates were generated assuming standard 3-flavour neutrino oscillation without the presence of any NSI effect. To do so, the standard oscillation parameter values have been fixed at their global best-fit point taken from ref. [23, 24]. For the test event rates, NSI has been considered with one parameter at a time. Test values of δ_{CP} and the NSI phase ϕ_{ij} for off-diagonal parameters ϵ_{ij} , with $i = e, \mu$; $j = \mu, \tau$ and $i \neq j$, have been varied in the range $[-180^\circ : 180^\circ]$. $\sin^2 \theta_{23}$ and $|\Delta_{31}|$ have been varied in the 3σ range taken from ref. [23, 24]. The off-diagonal NSI parameters $|\epsilon_{e\mu}|$, $|\epsilon_{\mu\tau}|$, and $|\epsilon_{e\tau}|$ have been varied in the range $[0 : 3]$, whereas the diagonal parameters $\epsilon_{\mu\mu}$ and $\epsilon_{\tau\tau}$ have been varied in the range $[-3 : 3]$. The marginalisation has been done over test values of δ_{CP} , $\sin^2 \theta_{23}$ and $|\Delta_{31}|$, along with the phases ϕ_{ij} in case of non-diagonal NSI parameters. The final results have been expressed as $\sqrt{\Delta\chi^2}$ as a function of test NSI parameters. It can be observed from the figure that in case of $\epsilon_{\mu\tau}$, all the 5 different runs can rule out $|\epsilon_{\mu\tau}| > 0.6$ at more than 20σ C.L. For the two diagonal terms, $\epsilon_{\mu\mu}$ and $\epsilon_{\tau\tau}$, all the different run schemes have almost equivalent sensitivity. For $\epsilon_{e\mu}$, and $\epsilon_{e\tau}$, however, the $5 + 5(\mu + e)$ run has much better sensitivity than the $5 + 5(\mu + \tau)$ or $5 + 5 + 1 + 1(\mu + \tau)$ runs. In table 2, we have given the expected 90% and 3σ constraints on different NSI parameters for different running schemes. It can be concluded that in case of $|\epsilon_{\mu\tau}|$, the $5 + 5 + 1 + 1(\mu + e + \tau)$ run has the best sensitivity among all the different running schemes. Also for $5 + 5 + 1 + 1(\mu + e + \tau)$ run, the 90% constraint of $|\epsilon_{\mu\tau}| < 7 \times 10^{-2}$ (6×10^{-2}) from DUNE will be close to the IceCube constraint of $|\epsilon_{\mu\tau}| < 2 \times 10^{-2}$ at 90% confidence level [39], if NH (IH) is the true hierarchy. $5 + 5(\mu + \tau)$ and $5 + 5 + 1 + 1(\mu + \tau)$ run has slightly weaker sensitivity than $5 + 5(\mu + e)$ run, but it is possible to provide complimentary sensitivity to $|\epsilon_{\mu\tau}|$ from the ν_τ and $\bar{\nu}_\tau$ appearance channels. In case of NSI due to $\epsilon_{\mu\mu}$, and $\epsilon_{\tau\tau}$ the $5 + 5(\mu + \tau)$ and $5 + 5 + 1 + 1(\mu + \tau)$ run schemes have sensitivities to NSI parameters of the similar order of magnitude as in other run schemes. For $|\epsilon_{\mu\tau}|$, the sensitivity is coming from ν_τ appearance and ν_μ disappearance channels, and the contribution from ν_e appearance channels are negligible. This is in agreement with the theoretical discussion given in section 2. From eq. B6 and B8 of ref. [36], it is clear that the sensitivity to $\epsilon_{\mu\mu}$ and $\epsilon_{\tau\tau}$ mostly comes from the muon disappearance channels due to their large statistics. For this reason, the sensitivity to $\epsilon_{\mu\mu}$ and $\epsilon_{\tau\tau}$ for the $\mu + \tau$ run schemes are comparable to the $\mu + e$ and $\mu + e + \tau$ run schemes. However, for $\epsilon_{e\mu}$ and $\epsilon_{e\tau}$, the $5 + 5(\mu + e)$ run has much better sensitivity compared to the run schemes without ν_e detection. We have presented the results for sensitivity to $\epsilon_{\mu\tau}$, $\epsilon_{\mu\mu}$ and $\epsilon_{\tau\tau}$ in fig. 18. The results for sensitivity to other two NSI parameters have been presented in the appendix C.

5 A short discussion on the unitarity of PMNS matrix and role of τ neutrino in determining it

One of the main physics motivation for the determination of τ neutrino is constraining the unitary property of the third row of the PMNS matrix. The unitary property of the PMNS matrix is broken when more than three neutrino generations exist in the nature.

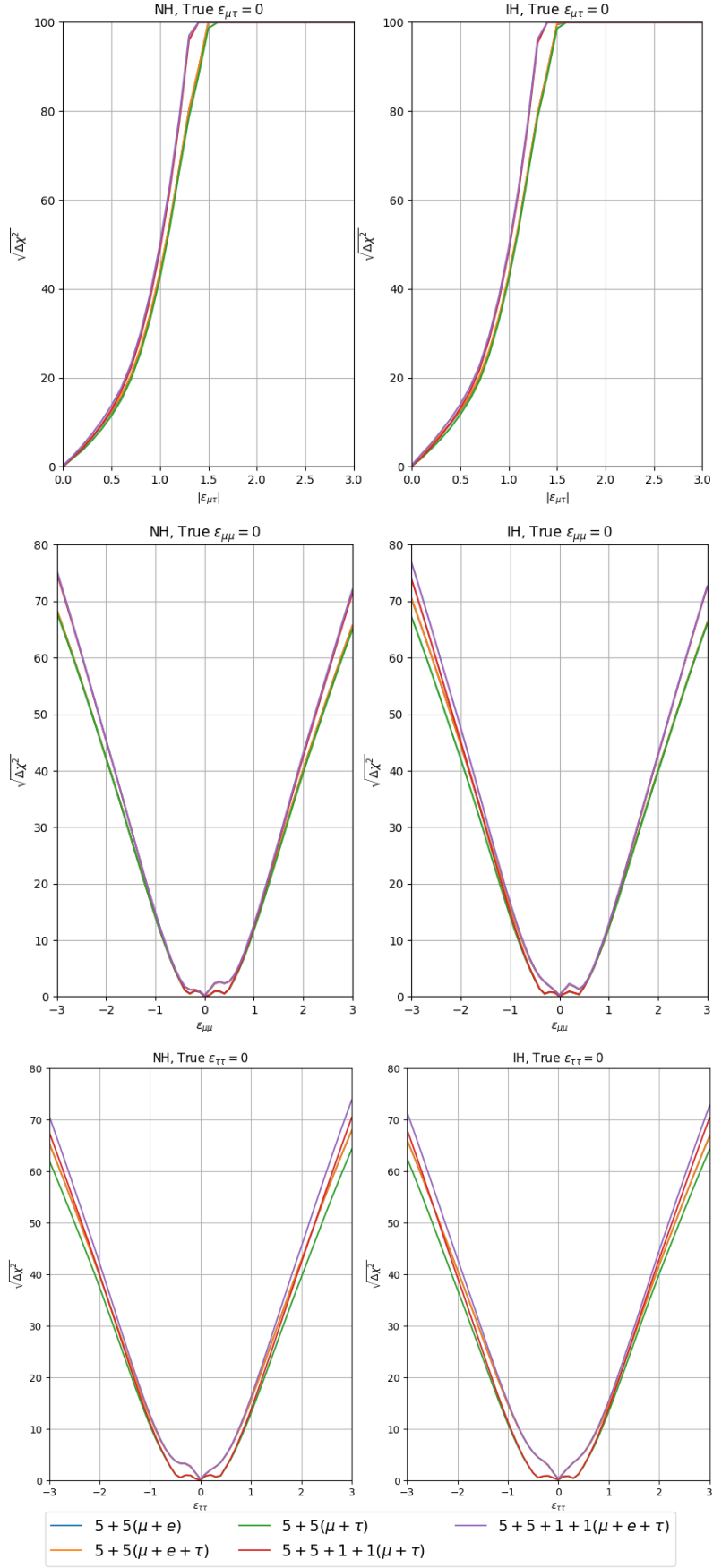


Figure 18. Sensitivity to NSI parameters $\epsilon_{\mu\tau}$, $\epsilon_{\mu\mu}$ and $\epsilon_{\tau\tau}$ with different runtimes of DUNE.

Parameters	5 + 5 ($\mu + e$)	5 + 5 ($\mu + \tau$)	5 + 5 ($\mu + e + \tau$)	5 + 5 + 1 + 1 ($\mu + \tau$)	5 + 5 + 1 + 1 ($\mu + e + \tau$)
$ \epsilon_{e\mu} $ NH	< 0.04 (0.10)	< 0.31 (0.43)	< 0.04 (0.10)	< 0.31 (0.43)	< 0.04 (0.10)
IH	< 0.04 (0.09)	< 0.25 (0.38)	< 0.04 (0.09)	< 0.25 (0.38)	< 0.04 (0.09)
$ \epsilon_{e\tau} $ NH	< 0.07 (0.20)	< 0.83 (1.02)	< 0.07 (0.20)	< 0.83 (1.02)	< 0.07 (0.20)
IH	< 0.09 (0.13)	< 0.78 (0.98)	< 0.09 (0.13)	< 0.78 (0.98)	< 0.09 (0.13)
$ \epsilon_{\mu\tau} $ NH	< 0.08 (0.14)	< 0.09 (0.17)	< 0.08 (0.14)	< 0.09 (0.15)	< 0.07 (0.13)
IH	< 0.07 (0.12)	< 0.10 (0.16)	< 0.07 (0.12)	< 0.09 (0.14)	< 0.06 (0.11)
$\epsilon_{\mu\mu}$ NH	> -0.40 (-0.50) < 0.11 (0.48)	> -0.43 (-0.50) < 0.50 (0.57)	> -0.40 (-0.50) < 0.11 (0.48)	> -0.43 (-0.50) < 0.50 (0.57)	> -0.40 (-0.50) < 0.11 (0.48)
IH	> -0.17 (-0.34) < 0.14 (0.56)	> -0.43 (-0.50) < 0.49 (0.54)	> -0.17 (-0.34) < 0.14 (0.56)	> -0.43 (-0.50) < 0.49 (0.54)	> -0.17 (-0.34) < 0.14 (0.56)
$\epsilon_{\tau\tau}$ NH	> -0.12 (-0.26) < 0.14 (0.35)	> -0.54 (-0.63) < 0.45 (0.51)	> -0.12 (-0.26) < 0.14 (0.35)	> -0.54 (-0.63) < 0.45 (0.51)	> -0.12 (-0.26) < 0.14 (0.35)
IH	> -0.11 (-0.20) < 0.09 (0.25)	> -0.51 (-0.60) < 0.42 (0.51)	> -0.11 (-0.20) < 0.09 (0.25)	> -0.51 (-0.60) < 0.42 (0.51)	> -0.11 (-0.20) < 0.09 (0.25)

Table 2. Expected 90% and 3σ constraints for 1 degree of freedom for different run times and for both the hierarchies. The 3σ constraints have been shown in the parenthesis.

A minimal model of extra 'sterile' neutrino consists of $3 + 1$ neutrino mixings dominated by the standard 3 flavours ν_e , ν_μ and ν_τ with a very small perturbative contribution from a new sterile flavour ν_s . ν_s consists, mainly, of a heavy mass eigenstate ν_4 with mass m_4 . If $m_1, m_2, m_3 \ll m_4$ and $\Delta_{41} = m_4^2 - m_1^2 = [0.1 - 10] \text{eV}^2$, then a direct sterile neutrino search in the neutrino oscillation experiments is possible. Recent results from the IceCube experiment constrain the sterile neutrino mass and mixing using atmospheric neutrino fluxes [46]. Constraints on the existence of sterile neutrino have been discussed in ref. [47–49], while ref. [50–54] discuss the effects of a light sterile neutrino on present and future long baseline experiments.

However, if the extra generation exists as iso-singlet neutral heavy leptons (NHL), then the sterile neutrinos will not take part in neutrino oscillations. In this case, their admixture in charged current weak interactions will violate the unitary property of the 3×3 mixing matrix. The 3-flavour neutrino oscillation will then be described by a non-unitary 3×3 mixing matrix. The non-unitary mixing matrix, in a generalised model independent way, can be written as

$$N = N_{NP} U_{3 \times 3} = \begin{bmatrix} \alpha_{00} & 0 & 0 \\ \alpha_{10} & \alpha_{11} & 0 \\ \alpha_{20} & \alpha_{21} & \alpha_{22} \end{bmatrix} U \quad (5.1)$$

where U is the PMNS matrix from eq. 1.1. The diagonal elements α_{ii} of N_{NP} are real, and the off-diagonal elements $\alpha_{ij} = |\alpha_{ij}|e^{i\phi_{ij}}$ are complex, with $i, j = 0, 1, 2$ and $i > j$. The constraints on the unitary properties of the first two rows of the mixing matrix can be given by detecting electron and $|\nu_\mu\rangle$ neutrinos at the neutrino oscillation experiments. However constraints on the third row mostly comes from charged lepton flavor violation (CLFV)

experiments. The present 3σ limits for 1 degree of freedom on the unitary violation in the third row of the mixing matrix from a joined fit of neutrino oscillation and CLFV (only neutrino oscillation) experiments are [16]:

$$|\alpha_{20}| < 4.4 \times 10^{-3} (9.8 \times 10^{-2}); |\alpha_{21}| < 2.0 \times 10^{-3} (1.7 \times 10^{-2}); \alpha_{22} > 0.9976 (0.76) \quad (5.2)$$

The opportunity to detect τ neutrinos and anti-neutrinos in DUNE gives a unique opportunity to constrain the violation of the unitary property of the third row of 3×3 mixing matrix through neutrino oscillation experiments. In ref. [55], it has been shown that tau neutrino appearance from the beam data at DUNE far detector, combined with the atmospheric data of ν_μ disappearance and ν_τ appearance can be useful to constrain the elements of the third row of the PMNS matrix. In fig. 19 we have shown the expected sensitivity to $|\alpha_{21}|$ and α_{22} from DUNE with different running schemes. We have not shown the sensitivity to α_{20} because the sensitivity is very low and that is because the $e - \tau$ oscillation is negligible in experiments with ν_μ and $\bar{\nu}_\mu$ beams. To calculate this sensitivity, we first obtained the true event rates considering standard 3×3 unitary mixing with the standard oscillation parameters fixed at the global best-fit values. For the test event rates, we varied $\sin^2 \theta_{23}$ and $|\Delta_{31}|$ in their 3σ ranges. δ_{CP} has been varied in the complete range $[-180^\circ : 180^\circ]$. The test mass hierarchy is same as the true one. The test values of the non-unitary parameter $|\alpha_{21}|$ (α_{22}) have been varied in the range $[0 : 0.1]$ ($[0.7 : 1]$). The phase ϕ_{21} associated with α_{21} has been varied in the range $[-180^\circ : 180^\circ]$. The $\Delta\chi^2$ between the true and test event rates have been calculated and marginalized over all the test parameters except $|\alpha_{21}|$ or α_{22} . It can be observed that for these two parameters, τ neutrino detection enhances the sensitivity of detecting these PMNS parameters. It can also be seen that $5 + 5(\mu + \tau)$ and $5 + 5 + 1 + 1(\mu + \tau)$ runs have better sensitivity than $5 + 5(\mu + e)$ run. The complete data set of the $5 + 5 + 1 + 1(\mu + e + \tau)$ run gives a 2σ limit of $|\alpha_{21}| < 0.1$ for both the hierarchies. This limit is weaker than the global limit from only neutrino oscillation given in eq. 5.2. For α_{22} , $5 + 5 + 1 + 1(\mu + e + \tau)$ run gives a 3σ limit of $\alpha_{22} > 0.83$ for both the hierarchies. This bound is stronger than the global limit from only neutrino oscillation data given in eq. 5.2.

6 Conclusions

In this work, we have investigated the impact of detecting ν_τ and $\bar{\nu}_\tau$ at DUNE on constraining Non-Standard Interactions (NSI) in neutrino propagation. We demonstrated that the most significant NSI effects on ν_τ appearance arise from $\epsilon_{\mu\tau}$, and that incorporating ν_τ detection alongside traditional ν_e and ν_μ channels improves sensitivity to this parameter. Our results indicate that DUNE's ability to probe $\epsilon_{\mu\tau}$ approaches the current constraint from IceCube, making ν_τ detection a valuable addition to NSI studies.

The three main physics goals of DUNE- namely, mass hierarchy determination, CP violation determination, and octant determination- are not affected by tau neutrino detection regardless of whether NSI effects are present or not. Although, we see that at the oscillation probability level, there are distinctions between two hierarchies for $|\epsilon_{\mu\tau}|$, the hierarchy sensitivity of ν_τ and $\bar{\nu}_\tau$ appearance channels is lost due to the $\phi_{\mu\tau}$ -hierarchy

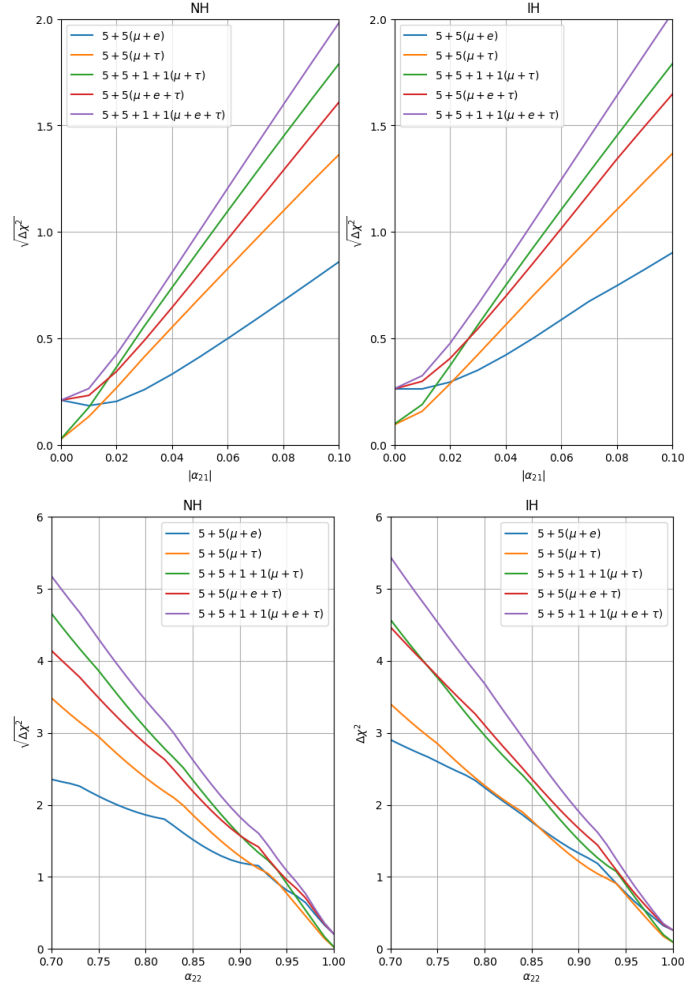


Figure 19. Sensitivity to non-unitary mixing parameters with different runtimes of DUNE.

degeneracy arising due to the dependency of the hierarchy sensitive term in the probability expression on $\cos \phi_{\mu\tau}$. For any true hierarchy and true value of $\phi_{\mu\tau}$, $P_{\mu\tau}$ and $P_{\bar{\mu}\bar{\tau}}$ can be mimicked by the wrong hierarchy and $\phi_{\mu\tau}(\text{test}) = 180^\circ - \phi_{\mu\tau}(\text{true})$.

For the same $\cos \phi$ dependent term, we found that the measurement of the NSI phase $\phi_{\mu\tau}$ can be enhanced through ν_τ detection, providing a potential additional source of CP violation. This is especially relevant in scenarios where the mass hierarchy is well-determined. The detection of τ neutrino appearances, along with μ neutrino disappearances, provide sensitivities to NSI parameters $\epsilon_{\mu\mu}$ and $\epsilon_{\tau\tau}$ which are comparable to the sensitivities from electron neutrino appearances and μ neutrino disappearances. The sensitivities to $\epsilon_{\mu\mu}$ and $\epsilon_{\tau\tau}$ mostly come from ν_μ and $\bar{\nu}_\mu$ disappearances. In case of $|\epsilon_{\mu\tau}|$, the $5+5+1+1(\mu+e+\tau)$ run provides a slightly stronger constraint than the $5+5(\mu+e)$ run. The constraint on $|\epsilon_{\mu\tau}|$ from the $5+5+1+1(\mu+\tau)$ run is close to the IceCube constraint [39]. This sensitivity to $|\epsilon_{\mu\tau}|$ comes from both muon disappearance and tau appearance channels. For the other two NSI parameter, considered in this paper, the $5+5(\mu+e)$ case has much better sensitivity

than any other running scheme without electron neutrino and anti-neutrino appearances. Therefore, in case of $\epsilon_{\mu\tau}$, $\epsilon_{\mu\mu}$ and $\epsilon_{\tau\tau}$, it is possible to obtain an independent complementary sensitivity by analysing the tau (anti-)neutrino appearance and muon (anti-)neutrino disappearance data alone.

Furthermore, we explored the implications of ν_τ detection for testing the unitarity of the PMNS matrix. The ability to constrain the non-unitary parameter α_{22} stronger than the present global fit limit using ν_τ appearance data presents an additional motivation for incorporating ν_τ measurements in DUNE experiments.

Looking ahead, our results suggest that future long-baseline and atmospheric neutrino experiments, such as DUNE, IceCube, and KM3NeT, could provide complementary constraints on NSI from ν_τ and $\bar{\nu}_\tau$ appearance channels. A combined analysis incorporating ν_τ data from these experiments may significantly enhance the sensitivity to $\epsilon_{\mu\tau}$ and other NSI parameters. Additionally, improvements in ν_τ identification at DUNE, such as optimized flux configurations and enhanced event reconstruction techniques, could further strengthen the experimental reach.

In conclusion, our study highlights the importance of ν_τ detection as a complementary probe of new physics in neutrino oscillations. Future experimental efforts aimed at increasing ν_τ detection efficiency will be crucial for refining NSI constraints and probing possible beyond Standard Model effects in the neutrino sector.

Acknowledgement

We thank Pedro Machado and Pedro Pasquini for the valuable discussions and comments over email communications. This work reflects the views of the authors and not those of the DUNE collaboration.

References

- [1] U. Rahaman, S. Razzaque and S.U. Sankar, *A Review of the Tension between the T2K and NOvA Appearance Data and Hints to New Physics*, *Universe* **8** (2022) 109 [2201.03250].
- [2] NOvA collaboration, *The NOvA Technical Design Report*, .
- [3] T2K collaboration, *The JHF-Kamioka neutrino project*, in *3rd Workshop on Neutrino Oscillations and Their Origin (NOON 2001)*, pp. 239–248, 6, 2001 [hep-ex/0106019].
- [4] T2K COLLABORATION collaboration, *Observation of Electron Neutrino Appearance in a Muon Neutrino Beam*, *Phys.Rev.Lett.* **112** (2014) 061802 [1311.4750].
- [5] T2K COLLABORATION collaboration, *Precise Measurement of the Neutrino Mixing Parameter θ_{23} from Muon Neutrino Disappearance in an Off-Axis Beam*, *Phys.Rev.Lett.* **112** (2014) 181801 [1403.1532].
- [6] J. Wolcott, “New oscillation results from nova with 10 years of data.” Talk given at the Neutrino 2024 meeting on June 17, 2024. Available at: <https://agenda.infn.it/event/37867/contributions/233955/attachments/121832/177712/2024-06-17%20Wolcott%20NOvA%202024%20results%20-%20NEUTRINO.pdf>, 2024.

- [7] U. Rahaman and S.K. Raut, *On the tension between the latest NO ν A and T2K data*, *Eur. Phys. J. C* **82** (2022) 910 [2112.13186].
- [8] U. Rahaman, *Looking for Lorentz invariance violation (LIV) in the latest long baseline accelerator neutrino oscillation data*, **2103.04576**.
- [9] L.S. Miranda, P. Pasquini, U. Rahaman and S. Razzaque, *Searching for non-unitary neutrino oscillations in the present T2K and NO ν A data*, *Eur. Phys. J. C* **81** (2021) 444 [1911.09398].
- [10] S.S. Chatterjee and A. Palazzo, *Nonstandard Neutrino Interactions as a Solution to the NO ν A and T2K Discrepancy*, *Phys. Rev. Lett.* **126** (2021) 051802 [2008.04161].
- [11] P.B. Denton, J. Gehrlein and R. Pestes, *CP -Violating Neutrino Nonstandard Interactions in Long-Baseline-Accelerator Data*, *Phys. Rev. Lett.* **126** (2021) 051801 [2008.01110].
- [12] DUNE collaboration, *The DUNE Far Detector Interim Design Report Volume 1: Physics, Technology and Strategies*, **1807.10334**.
- [13] HYPER-KAMIOKANDE WORKING GROUP collaboration, *T2HK: J-PARC upgrade plan for future and beyond T2K*, in *15th International Workshop on Neutrino Factories, Super Beams and Beta Beams*, 11, 2013 [1311.5287].
- [14] A. Friedland and I.M. Shoemaker, *Searching for Novel Neutrino Interactions at NO ν A and Beyond in Light of Large θ_{13}* , **1207.6642**.
- [15] S.-F. Ge, P. Pasquini, M. Tortola and J.W.F. Valle, *Measuring the leptonic CP phase in neutrino oscillations with nonunitary mixing*, *Phys. Rev.* **D95** (2017) 033005 [1605.01670].
- [16] F.J. Escrivuela, D.V. Forero, O.G. Miranda, M. Tórtola and J.W.F. Valle, *Probing CP violation with non-unitary mixing in long-baseline neutrino oscillation experiments: DUNE as a case study*, *New J. Phys.* **19** (2017) 093005 [1612.07377].
- [17] D. Kaur, N.R. Khan Chowdhury and U. Rahaman, *Effect of non-unitary mixing on the mass hierarchy and CP violation determination at the Protvino to ORCA experiment*, *Eur. Phys. J. C* **84** (2024) 118 [2110.02917].
- [18] S.S. Chatterjee and A. Palazzo, *Status of tension between NO ν A and T2K after Neutrino 2024 and possible role of non-standard neutrino interactions*, **2409.10599**.
- [19] A. De Gouvêa, K.J. Kelly, G.V. Stenico and P. Pasquini, *Physics with Beam Tau-Neutrino Appearance at DUNE*, *Phys. Rev. D* **100** (2019) 016004 [1904.07265].
- [20] P. Machado, H. Schulz and J. Turner, *Tau neutrinos at DUNE: New strategies, new opportunities*, *Phys. Rev. D* **102** (2020) 053010 [2007.00015].
- [21] M. Masud, M. Bishai and P. Mehta, *Extricating New Physics Scenarios at DUNE with Higher Energy Beams*, *Sci. Rep.* **9** (2019) 352 [1704.08650].
- [22] A. Ghoshal, A. Giarnetti and D. Meloni, *On the role of the ν_τ appearance in DUNE in constraining standard neutrino physics and beyond*, *JHEP* **12** (2019) 126 [1906.06212].
- [23] I. Esteban, M.C. Gonzalez-Garcia, M. Maltoni, I. Martinez-Soler, J.a.P. Pinheiro and T. Schwetz, *NuFit-6.0: Updated global analysis of three-flavor neutrino oscillations*, **2410.05380**.
- [24] Nufit6.0 <http://www.nu-fit.org/?q=node/294>, 2024.
- [25] P.B. Denton, H. Minakata and S.J. Parke, *Compact Perturbative Expressions For Neutrino Oscillations in Matter*, *JHEP* **06** (2016) 051 [1604.08167].

- [26] Y. Farzan and M. Tortola, *Neutrino oscillations and Non-Standard Interactions*, *Front. in Phys.* **6** (2018) 10 [[1710.09360](#)].
- [27] C. Biggio, M. Blennow and E. Fernandez-Martinez, *General bounds on non-standard neutrino interactions*, *JHEP* **08** (2009) 090 [[0907.0097](#)].
- [28] T. Ohlsson, *Status of non-standard neutrino interactions*, *Rept. Prog. Phys.* **76** (2013) 044201 [[1209.2710](#)].
- [29] O.G. Miranda and H. Nunokawa, *Non standard neutrino interactions: current status and future prospects*, *New J. Phys.* **17** (2015) 095002 [[1505.06254](#)].
- [30] *Neutrino Non-Standard Interactions: A Status Report*, vol. 2, 2019. 10.21468/SciPostPhysProc.2.001.
- [31] Y. Farzan, *A model for large non-standard interactions of neutrinos leading to the LMA-Dark solution*, *Phys. Lett. B* **748** (2015) 311 [[1505.06906](#)].
- [32] Y. Farzan and I.M. Shoemaker, *Lepton Flavor Violating Non-Standard Interactions via Light Mediators*, *JHEP* **07** (2016) 033 [[1512.09147](#)].
- [33] L. Wolfenstein, *Neutrino oscillations in matter*, *Phys. Rev.* **D17** (1978) 2369.
- [34] S.P. Mikheev and A.Y. Smirnov, *Resonance Amplification of Oscillations in Matter and Spectroscopy of Solar Neutrinos*, *Sov. J. Nucl. Phys.* **42** (1985) 913.
- [35] S.P. Mikheev and A.Y. Smirnov, *Resonant amplification of neutrino oscillations in matter and solar neutrino spectroscopy*, *Nuovo Cim.* **C9** (1986) 17.
- [36] T. Kikuchi, H. Minakata and S. Uchinami, *Perturbation Theory of Neutrino Oscillation with Nonstandard Neutrino Interactions*, *JHEP* **03** (2009) 114 [[0809.3312](#)].
- [37] I. Martinez-Soler and H. Minakata, *Standard versus Non-Standard CP Phases in Neutrino Oscillation in Matter with Non-Unitarity*, *PTEP* **2020** (2020) 063B01 [[1806.10152](#)].
- [38] M.E. Chaves, D.R. Gratieri and O.L.G. Peres, *Improvements on perturbative oscillation formulas including non-standard neutrino interactions*, *J. Phys. G* **48** (2020) 015001 [[1810.04979](#)].
- [39] (ICECUBE COLLABORATION)*, ICECUBE collaboration, *All-flavor constraints on nonstandard neutrino interactions and generalized matter potential with three years of IceCube DeepCore data*, *Phys. Rev. D* **104** (2021) 072006 [[2106.07755](#)].
- [40] P. Coloma, I. Esteban, M.C. Gonzalez-Garcia and M. Maltoni, *Improved global fit to Non-Standard neutrino Interactions using COHERENT energy and timing data*, *JHEP* **02** (2020) 023 [[1911.09109](#)].
- [41] T2K collaboration, *Measurement of neutrino and antineutrino oscillations by the T2K experiment including a new additional sample of ν_e interactions at the far detector*, *Phys. Rev.* **D96** (2017) 092006 [[1707.01048](#)].
- [42] DUNE collaboration, *Experiment Simulation Configurations Approximating DUNE TDR*, [2103.04797](#).
- [43] DUNE tau optimized fluxes. Available at: <https://glaucus.crc.nd.edu/DUNEFluxes/>.
- [44] P. Huber, M. Lindner and W. Winter, *Simulation of long-baseline neutrino oscillation experiments with GLOBES (General Long Baseline Experiment Simulator)*, *Comput.Phys.Commun.* **167** (2005) 195 [[hep-ph/0407333](#)].

- [45] P. Huber, J. Kopp, M. Lindner, M. Rolinec and W. Winter, *New features in the simulation of neutrino oscillation experiments with GLoBES 3.0: General Long Baseline Experiment Simulator*, *Comput.Phys.Commun.* **177** (2007) 432 [[hep-ph/0701187](#)].
- [46] ICeCUBE collaboration, *Searches for Sterile Neutrinos with the IceCube Detector*, *Phys. Rev. Lett.* **117** (2016) 071801 [[1605.01990](#)].
- [47] D.A. Bryman and R. Shrock, *Constraints on Sterile Neutrinos in the MeV to GeV Mass Range*, [1909.11198](#).
- [48] S. Böser, C. Buck, C. Giunti, J. Lesgourgues, L. Ludhova, S. Mertens et al., *Status of Light Sterile Neutrino Searches*, [1906.01739](#).
- [49] L.S. Miranda and S. Razzaque, *Revisiting constraints on $3 + 1$ active-sterile neutrino mixing using IceCube data*, *JHEP* **03** (2019) 203 [[1812.00831](#)].
- [50] S. Gupta, Z.M. Matthews, P. Sharma and A.G. Williams, *The Effect of a Light Sterile Neutrino at NO ν A and DUNE*, *Phys. Rev.* **D98** (2018) 035042 [[1804.03361](#)].
- [51] A. Chatla, S. Rudrabhatla and B.A. Bambah, *Degeneracy Resolution Capabilities of NO ν A and DUNE in the Presence of Light Sterile Neutrino*, *Adv. High Energy Phys.* **2018** (2018) 2547358 [[1804.02818](#)].
- [52] S. Choubey, D. Dutta and D. Pramanik, *Measuring the Sterile Neutrino CP Phase at DUNE and T2HK*, *Eur. Phys. J.* **C78** (2018) 339 [[1711.07464](#)].
- [53] S. Choubey, D. Dutta and D. Pramanik, *Imprints of a light Sterile Neutrino at DUNE, T2HK and T2HKK*, *Phys. Rev.* **D96** (2017) 056026 [[1704.07269](#)].
- [54] J.M. Berryman, A. de Gouvêa, K.J. Kelly and A. Kobach, *Sterile neutrino at the Deep Underground Neutrino Experiment*, *Phys. Rev.* **D92** (2015) 073012 [[1507.03986](#)].
- [55] P.B. Denton and J. Gehrlein, *New oscillation and scattering constraints on the tau row matrix elements without assuming unitarity*, *JHEP* **06** (2022) 135 [[2109.14575](#)].

A More discussions on fluxes and detector simulations

In section 1, we mentioned that although ref. [19, 21, 22] discussed about the role of tau neutrino detection in the NSI analysis at DUNE, all of them had considered outdated fluxes. In fig. 20, we have shown the comparison between the fluxes used in our paper (referred to as "new"), and those used in the previous works (referred to as "old"). We can see that for the regular DUNE beam, the fluxes used in our paper are significantly higher than those used in previous works, and hence the former lead to higher statistics than the latter. The tau optimized fluxes in both the cases are almost equivalent. For ν_μ disappearances, and ν_e appearances, ref. [19, 21, 22] have used the detector simulations provided in ref. [?], whereas we have used the detector simulations provided in ref. [42]. For the tau optimized fluxes, we have followed the simulations provided in ref. [19]. However, they did not use tau optimized anti-neutrino beam. In section 3, we have discussed the details of the simulations for tau optimized anti-neutrino beam. Ref. [22] used a different simulation for their tau optimized beam. For instance, they considered a constant efficiency independent of energy for all the energy bins, whereas we have considered energy dependent efficiencies for each

energy bin. Details of the energy resolution functions for the tau neutrino and anti-neutrino appearance channels have not been provided in ref. [22].

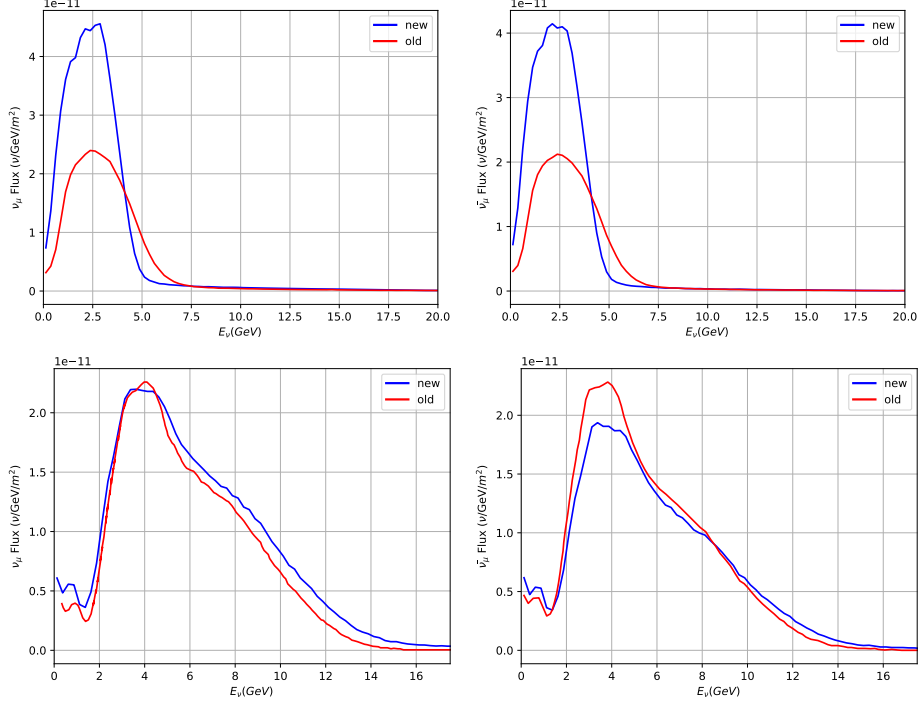


Figure 20. Comparison between fluxes used in our paper with those used in previous works. The top (bottom) panels are for the regular (tau optimized) fluxes, and the left (right) panels are for ν_μ ($\bar{\nu}_\mu$) fluxes in the neutrino (anti-neutrino) beam.

B Octant sensitivity for NSI due to $\epsilon_{\mu\tau}$, $\epsilon_{\mu\mu}$ and $\epsilon_{\tau\tau}$

We have discussed about the octant sensitivity from τ neutrino and anti-neutrino appearance channels in presence of NSI in section 4.3. In fig. 16, we presented the results for NSI due to $\epsilon_{e\mu}$, and $\epsilon_{e\tau}$ only. In this section, we will present the octant sensitivity results for other three NSI parameters, namely $\epsilon_{\mu\tau}$, $\epsilon_{\mu\mu}$ and $\epsilon_{\tau\tau}$ in fig. 21. $5 + 5(\mu + \tau)$, $5 + 5 + 1 + 1(\mu + \tau)$ running schemes do not have any octant sensitivity for these three NSI parameters. $5 + 5(\mu + e)$ run has good octant sensitivity but it does not improve with additional data from ν_τ and $\bar{\nu}_\tau$ appearance channels.

C Sensitivity to $\epsilon_{e\mu}$ and $\epsilon_{e\tau}$

In section 4.5, we have discussed the sensitivity to different NSI parameters. In fig. 18, we have presented the results for sensitivity to NSI parameters for $\epsilon_{\mu\tau}$, $\epsilon_{\mu\mu}$ and $\epsilon_{\tau\tau}$. The results for sensitivity to $\epsilon_{e\mu}$ and $\epsilon_{e\tau}$ have been represented in fig. 22.

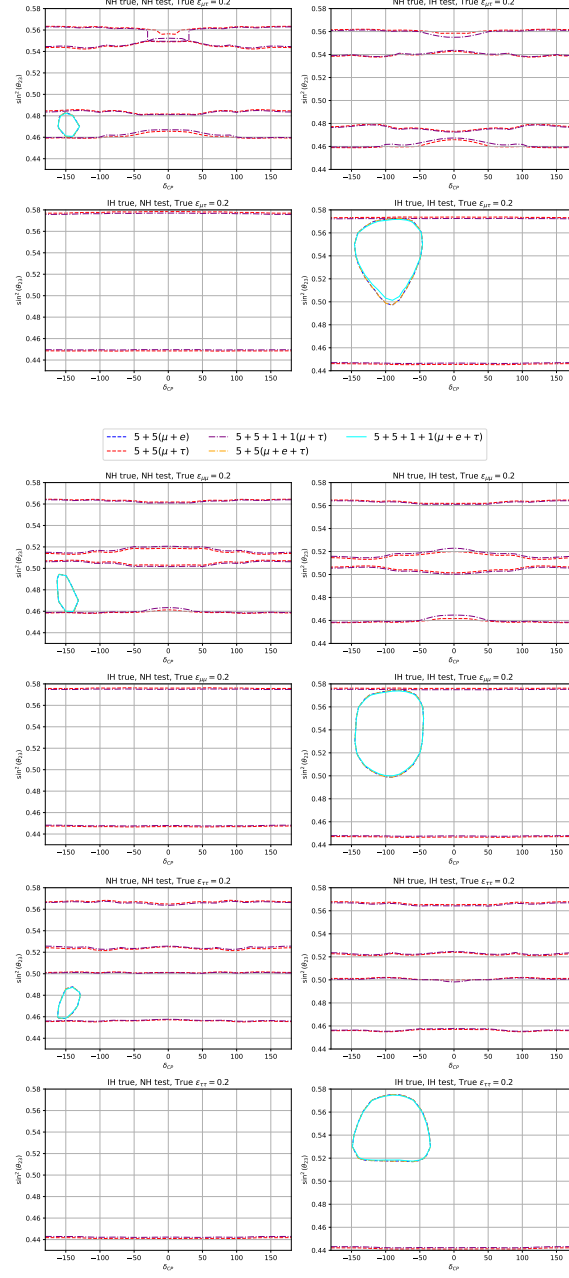


Figure 21. Allowed regions in the test $\delta_{CP} - \sin^2\theta_{23}$ plane for oscillation with NSI due to $\epsilon_{\mu\tau}$, $\epsilon_{\mu\mu}$ and $\epsilon_{\tau\tau}$. The top (bottom) panels are for NH (IH) being the true hierarchy. The left (right) panels are for test hierarchy being NH (IH).

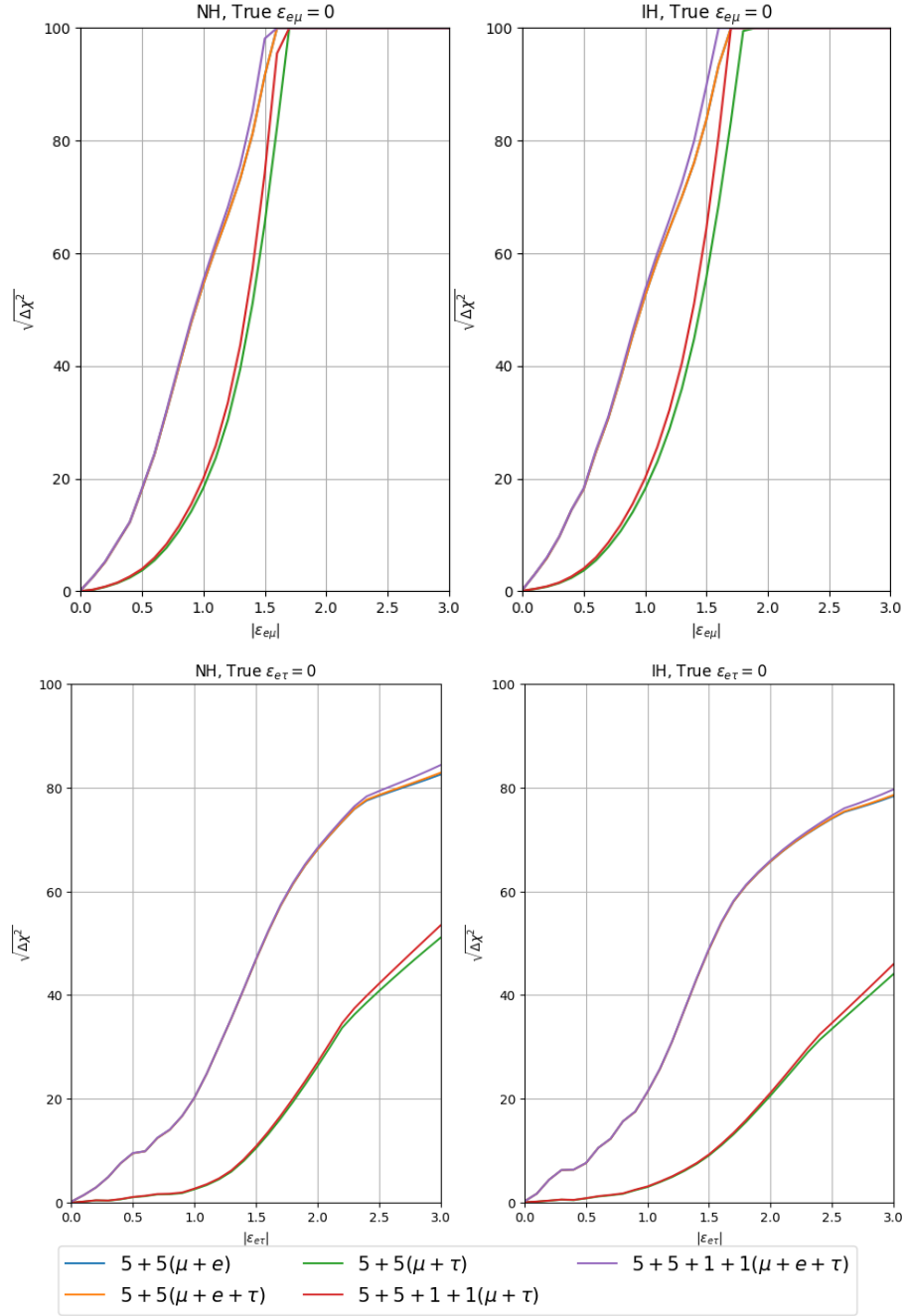


Figure 22. Sensitivity to different NSI parameters $\epsilon_{e\mu}$ and $\epsilon_{e\tau}$ with different runtimes of DUNE.